Amplified Fluorescence in Situ Hybridization by Small and Bright Dye-Loaded Polymeric Nanoparticles

Sylvie Egloff, Nina Melnychuk, Elisabete Cruz da Silva, Andreas Reisch, Sophie Martin, Andrey S Klymchenko

ACSNANO

www.acsnano.org

ARTICLE

Amplified Fluorescence *in Situ* Hybridization by Small and Bright Dye-Loaded Polymeric Nanoparticles

Sylvie Egloff,[§] Nina Melnychuk,[§] Elisabete Cruz Da Silva, Andreas Reisch, Sophie Martin, and Andrey S. Klymchenko*

Cite This: https://doi.org/10.1021/acsnano.1c09409

Read Online

ACCESS | Metrics & More | Article Recommendations | Supporting Information

ABSTRACT: **Detection and imaging of RNA at the single-cell level is of utmost importance for fundamental research and clinical diagnostics. Current techniques of RNA analysis, including fluorescence *in situ* hybridization (FISH), are long, complex, and expensive. Here, we report a methodology of amplified FISH (AmpliFISH) that enables simpler and faster RNA imaging using small and ultrabright dye-loaded polymeric nanoparticles (NPs) functionalized with DNA. We found that the small size of NPs (below 20 nm) was essential for their access to the intracellular mRNA targets in fixed permeabilized cells. Moreover, proper selection of the polymer matrix of DNA-NPs minimized nonspecific intracellular interactions. Optimized DNA-NPs enabled sequence-specific imaging of different mRNA targets (survivin, actin, and polyA tails), using a simple 1 h staining protocol. Encapsulation of cyanine and rhodamine dyes with bulky counterions yielded green-, red-, and far-red-emitting NPs that were 2−100-fold brighter than corresponding quantum dots. These NPs enabled multiplexed detection of three mRNA targets simultaneously, showing distinctive mRNA expression profiles in three cancer cell lines. Image analysis confirmed the single-particle nature of the intracellular signal, suggesting single-molecule sensitivity of the method. AmpliFISH was found to be semiquantitative, correlating with RT-qPCR. In comparison with the commercial locked nucleic acid (LNA)-based FISH technique, AmpliFISH provides 8−200-fold stronger signal (dependent on the NP color) and requires only three steps *vs* ∼20 steps together with a much shorter time. Thus, combination of bright fluorescent polymeric NPs with FISH yields a fast and sensitive single-cell transcriptomic analysis method for RNA research and clinical diagnostics.**

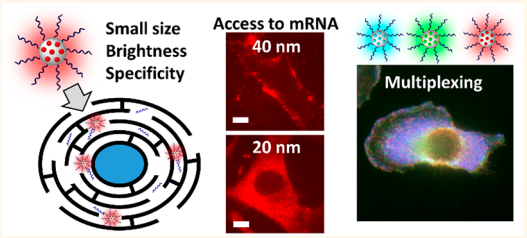

KEYWORDS: *fluorescent nanoparticles, DNA-functionalized polymeric nanoparticles, fluorescence in situ hybridization, single-cell analysis, RNA imaging, mRNA, fluorescence microscopy*

With the ever-growing role of RNA in understanding and controlling cellular processes,[1,2] detection and imaging of intracellular RNA attract significant attention.[3−5] Current approaches include fluorescence *in situ* hybridization (FISH),[6] single-cell RNA sequencing,[7,8] and molecular biology techniques based on labeled RNA-binding proteins[4,9] and light-up aptamers.[10−14] *In situ* hybridization, introduced more than 50 years ago,[15,16] and its fluorescence version FISH[17,18] are particularly suitable for imaging native nucleic acids within cells and tissues, with applications ranging from fundamental RNA research to clinical diagnostics.[6,19] In particular, RNA-FISH, which allows spatial and temporal monitoring of intracellular RNA, provides important insights into mechanisms of transcription and translation[20,21] and serves as a tool for cell-based diagnostics.[22,23] Advanced versions of RNA-FISH, developed in the last decades, enable detection and quantification of intracellular RNA with single-molecule sensitivity.[24−27] Nevertheless, broad applications of RNA-FISH in research and clinical diagnostics are still limited by a number of challenges. In particular, low-abundant RNA are still difficult to identify,[28] because of limited fluorescence signal provided by single organic dye molecules. Therefore, many approaches have been developed to amplify the fluorescence signal, such as branched DNA amplification,[29−31] different isothermal amplification strategies,[32] rolling circle amplification (RPA),[33] hybridization chain reaction (HCR),[34,35] primer-exchange reaction,[36,37] and click-amplifying FISH (Clamp-FISH).[38] The signal amplification can be also achieved by using

Received: October 24, 2021
Accepted: December 14, 2021

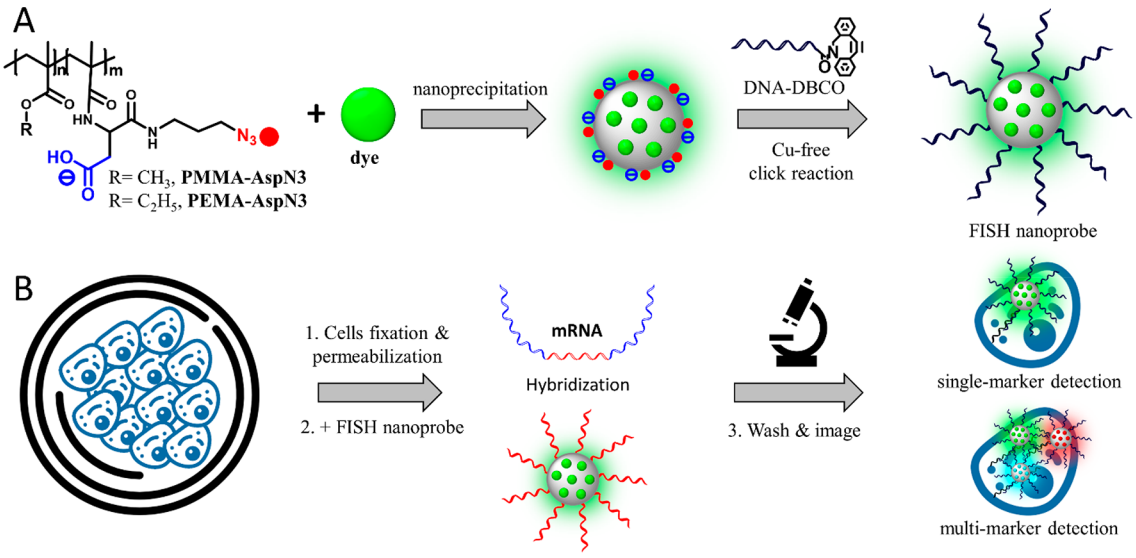

Figure 1. Principle of AmpliFISH using DNA-functionalized dye-loaded polymeric NPs. (A) Design of FISH nanoprobes based on polymeric nanoparticles. (B) Workflow for detection of target mRNA in fixed and permeabilized cells.

multiple singly labeled oligonucleotides (generally 30−48) that hybridize along the same target RNA transcript,[27] known as the Stellaris FISH method.[39] However, FISH techniques include complicated time-consuming procedures with multiple steps and require experienced staff, which make development of validated protocols for clinics very expensive.[40] Moreover, FISH protocols are probe- and sample-dependent and have to be optimized for each set of conditions.[41]

Fluorescent probes based on nanoparticles (NPs) can potentially overcome some of the limitations in the field of nucleic acid detection.[42] In particular, high fluorescence brightness of NPs may allow direct detection of the biomolecular targets without the need of complex and time-consuming amplification protocols.[43−48] NPs can provide fluorescence signal amplification for nucleic acid detection using different mechanisms, including energy transfer from semiconductor quantum dots[49] and polymeric NPs[50−52] as well as plasmonics-based fluorescence enhancement,[53,54] hybridization-triggered molecular assembly,[55] *etc.* Direct intracellular detection of nucleic acids by NPs inside the cells is a highly attractive approach,[56] and a few reported examples include gold nanoparticles (nanoflares)[57−59] DNA-based nanostructures,[60−63] semiconductor quantum dots,[64,65] upconversion NPs,[66] carbon nanostructures,[67,68] as well as lipid NPs,[69,70] polymeric NPs,[71] hybrid organic−inorganic NPs,[72] *etc.* However, RNA detection in live cells remains complicated by efficient endocytosis of nanomaterials with their potential degradation by enzymes and generic problem of endosomal escape of entrapped NPs.[73−75] In this respect, the combination of the FISH technique in fixed and permeabilized cells with luminescent NPs is of particular interest, because it can ensure direct access of NPs to the target RNA and take advantage of established FISH protocols in biological and clinical applications.[19] However, this possibility was realized only recently using semiconductor quantum dots (QDs) in combination with the Stellaris approach, where distinct mRNA transcripts have been detected and quantified at the single-molecule level in individual cells.[65] To achieve this, the authors specially designed compact QDs, which could better access the whole cytosol and thus hybridize with the intracellular mRNA.[65]

Dye-loaded polymeric nanoparticles, which have attracted attention in recent years due to their high brightness and modularity,[45,76] could be a promising platform for development of a simple and rapid RNA-FISH probes. To address the problem of aggregation-caused quenching of encapsulated dyes in these NPs, we proposed a concept of ionic dye insulation by bulky hydrophobic counterions, yielding NPs 6−100-fold brighter than corresponding QDs.[52,77,78] The size of these NPs can be tuned from 10 to 50 nm depending on the nature of the polymer,[79] which is a critical point because NPs should be able to reach the RNA target within the cytosol.[65] Indeed, polymeric NPs with sizes of <23 nm are required to diffuse and spread in the cytosol of living cells.[80] In addition to rhodamine dye, cyanine dyes can also be encapsulated to prepare NPs of any desired color, which was applied for multicolor barcoding of live cells and for long-term tracking *in vitro* and *in vivo*.[81] Moreover, the efficient energy transfer within donor dyes inside the NPs can generate a giant light-harvesting antenna that amplifies the fluorescence signal of an single acceptor >1000-fold.[82] Their functionalization with oligonucleotides yielded nanoprobes for amplified detection of DNA and RNA in solutions with a picomolar limit of detection[52] and on surfaces with single-molecule sensitivity[51] and compatibility with mobile phone cameras.[83] These DNA-functionalized NPs have already been validated for detection of microRNA in cell extracts,[84] but they have not been explored to date for direct detection of RNA inside the cells.

In the present work, we developed a methodology of amplified FISH (AmpliFISH) based on ultrabright dye-loaded polymeric NPs functionalized with DNA. In this approach, the hybridization AmpliFISH probe with the target mRNA inside the cells results in a fluorescence signal equivalent to 80−300 encapsulated dyes per single sequence, which ensures strong signal amplification. We show that the size of NPs < 16 nm was essential to achieve effective penetration of fixed cells and hybridization with the target. Owing to their high brightness, these FISH nanoprobes can detect target mRNA in fixed cells using a simple and rapid protocol (<3 h). Importantly, FISH nanoprobes of three different colors could be used simultaneously to target different RNA sequences. The methodology

https://doi.org/10.1021/acsnano.1c09409
ACS Nano XXXX, XXX, XXX−XXX

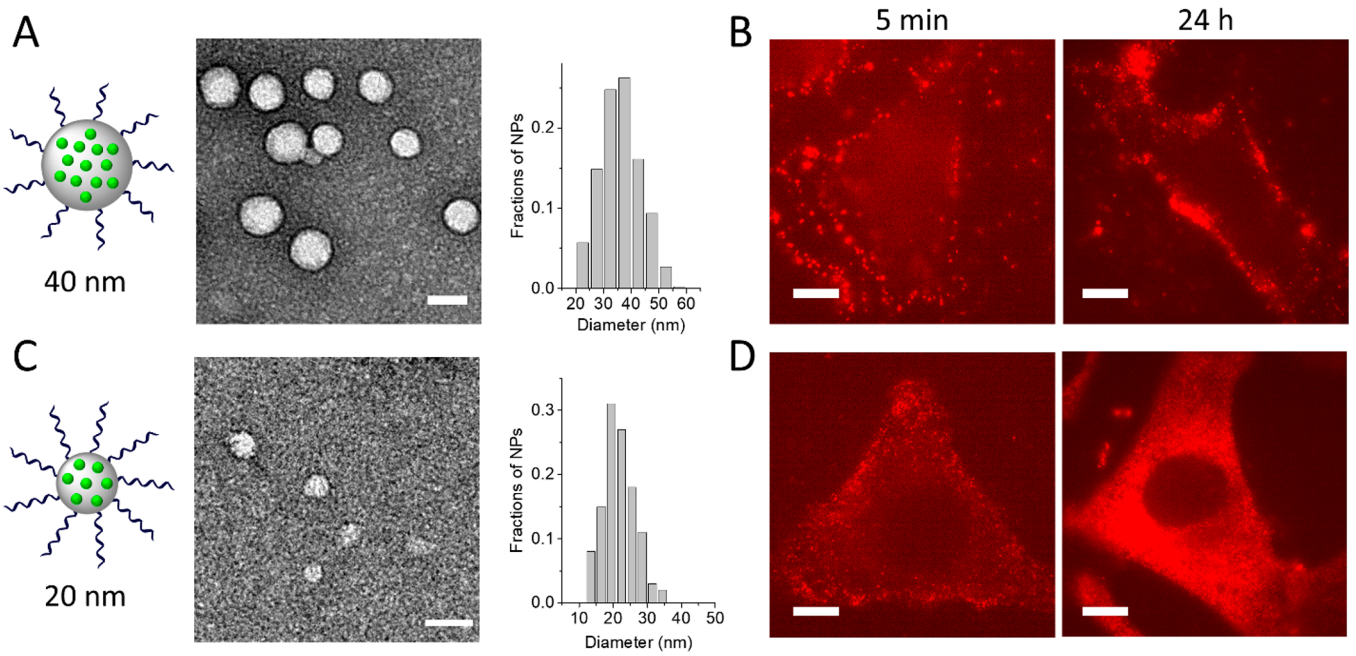

Figure 2. Testing DNA-functionalized NPs of two different sizes in fixed permeabilized HeLa cells. (A, C) NPs of two different average sizes of their core, ~40 nm (A) and ~20 nm (C), and their corresponding TEM images and size distribution histograms. (B, D) Fluorescence microscopy (TIRF) images of cells labeled for different times (5 min and 24 h) with DNA-NPs (T20-NPs) of two different sizes: ~40 nm (B) and ~20 nm (D). Scale bar is 10 μm.

was validated on three cancer cell lines, and it allows semiquantitative analysis of mRNA abundance. The developed probes and the FISH methodology can greatly simplify FISH-based imaging of RNA inside cells for both fundamental research and clinical diagnostics.

RESULTS AND DISCUSSION

Design and Optimization of FISH Nanoprobes. The design of our FISH nanoprobes is based on dye-loaded polymeric NPs functionalized with nucleic acids complementary to the mRNA target (Figure 1). Dye-loaded NPs are made of poly(methyl methacrylate) (PMMA) or poly(ethyl methacrylate) (PEMA) polymers bearing azide and a negatively charged carboxylate group (Figure 1A). Nanoprecipitation of these hydrophobic polymers with charged groups yields ultrasmall NPs, where the core is formed by the hydrophobic domain of the polymer, while the charged carboxylate exposes an azide group at the NP surface to ensure high reactivity for the click reaction.[51,52,85] For encapsulation, we used octadecyl rhodamine B R18 with its bulky hydrophobic counterion trakis-(pentafluorophenyl)borate (F5). The latter serves as an insulator that prevents the dyes from aggregation-caused quenching when loaded at high concentration and at the same time ensures effective encapsulation without dye leakage.[77,86] The dye-loaded NPs were obtained by nanoprecipitation of the polymer and the dye from acetonitrile into corresponding buffer. Then, oligonucleotides were grafted to the NPs' surface by reacting the exposed azide groups with DBCO groups of oligonucleotides (Figure 1A). The sequence of grafted oligonucleotides was a 20−22mer complementary to the target mRNA of actin and survivin. The former is a common housekeeping gene well expressed in many cell lines, while the latter is a common marker of cancer cells.[87] In our AmpliFISH technique, the NPs bearing capture sequences are expected to hybridize with the mRNA target inside the cells. For this purpose, the cells should be fixed and permeabilized (Figure 1B).

The key question here is the size of NPs required to penetrate the cells, diffuse freely through the labyrinth of the intracellular structures, and reach the target mRNA sequence.[65] Therefore, we first formulated dye-loaded NPs with different sizes. The larger particles (40 nm core size, Figure 2A) were based on a PMMA bearing 1.6% of charged groups (PMMA-AspN3-1.6%), the same as reported previously by us.[52] To obtain smaller NPs, we used PMMA with a larger number of charged groups (5%), which was shown to favor a decrease in the particle size obtained by nanoprecipitation.[51,80] The obtained NPs loaded with 30 wt % of R18/F5 displayed a 22 nm core size according to transmission electron microscopy (TEM, Figure 2C).

To verify whether the probes can enter fixed permeabilized cells and hybridize with mRNA, we first functionalized NPs with T20 DNA. They are expected to hybridize with all mRNA, because each mRNA bears a poly(A) tail at the 3′ end. After fixation and permeabilization, the cells were incubated with NPs (30 min), then washed and imaged using fluorescence microscopy. We found that larger NPs were unable to enter the fixed cells, as they all remained at the cell surface even after 24 h of incubation with NPs (Figure 2B). In sharp contrast, smaller NPs showed intracellular fluorescence already after 5 min of incubation and then a strong intracellular signal after 24 h (Figure 2D). Thus, we could conclude that NPs of small size are required for the design of the FISH probe, which is in line with the earlier report based on QDs.[65] Our earlier works on live cells also showed that small size (<23 nm) was essential for free diffusion of NPs inside the cytosol.[80]

Then, we tested whether the hybridization with the poly(A) tails is specific. We replaced T20 DNA with A20 DNA, which is not expected to hybridize with the poly(A) targets. However, microscopy experiments showed that the intracellular signal for these NPs remained high, indicating strong nonspecific

https://doi.org/10.1021/acsnano.1c09409
ACS Nano XXXX, XXX, XXX−XXX

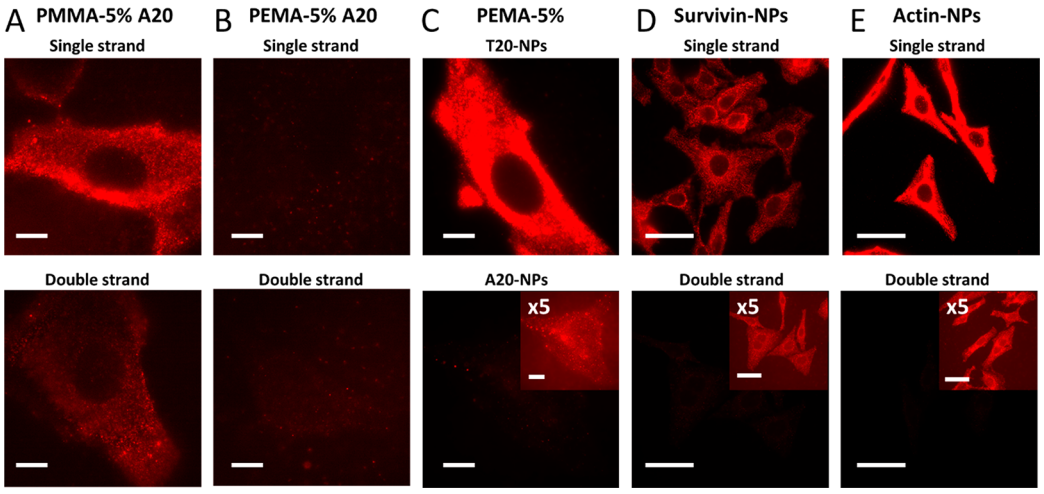

Figure 3. Effect of polymer nature and different grafted DNA sequences. (A, B) Fluorescence images of fixed HeLa cells incubated with PMMA-based NPs (A) and PEMA-based NPs (B) of ∼20 nm core size, functionalized with A20. Both single-stranded and double-stranded (annealed with T20) DNA NPs were tested (30 min incubation with cells). TIRF mode was used on fixed HeLa cells without washing. (C) Comparison of TIRF fluorescence images of PEMA-based NPs functionalized with T20 (upper panel) and A20 (lower panel) recorded at identical conditions (inset shows an image where the signal was amplified 5-fold for visibility of the cell). Cells were incubated during 1 h with NPs, then washed two times with 0.1% BSA/PBS. Scale bar: 10 μm. (D, E) Epi-fluorescence microscopy of fixed HeLa cells incubated for 1 h with DNA-NPs targeting survivin and β-actin (the same washing protocol as in C). Images for single-stranded (upper panels) and double-stranded (annealed with complementary strands) DNA-NPs are shown. Scale bar: 50 μm. PBS buffer with 50 mg/L Tween 80 was systematically used for incubation and imaging (A–E).

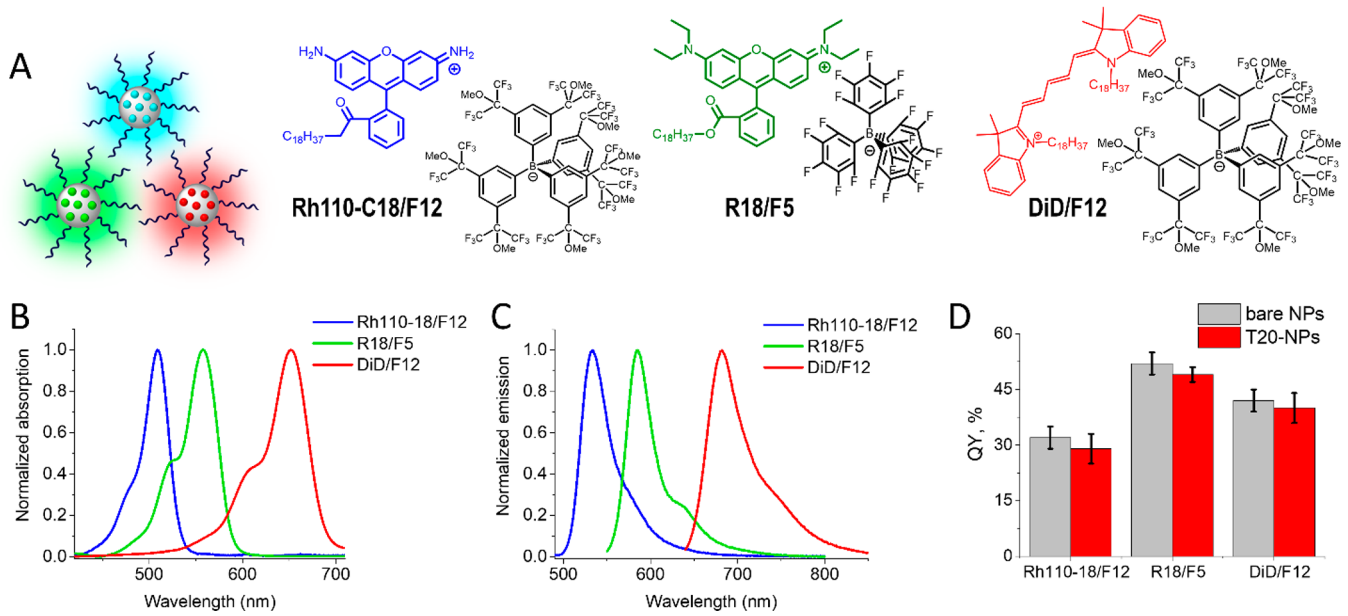

Figure 4. FISH-NPs of three different colors. (A) Dye salts with bulky counterions used for encapsulation into polymeric NPs. (B) Absorption and (C) fluorescence spectra of DNA-NP loading three different dye salts. (D) Fluorescence quantum yields of bare NPs and DNA-NPs (T20 oligonucleotide). Dye loading (weight % ratio with respect to the polymer) was 30 wt %. Error bars are standard deviation ($n \geq 3$).

f3

interactions of NPs inside the cells (Figure 3A). We further annealed the A20-functionalized NPs with T20 DNA to obtain double-stranded oligonucleotides at the NP surface. In this case, the intracellular signal decreased (Figures 3A and S1), but still remained significant, confirming the nonspecific interactions of NPs with the cells, independent from the DNA/RNA hybridization. Therefore, we formulated small NPs based on another polymer, PEMA bearing 5% charged groups (PEMA-MA-5%), which was previously shown to yield ∼20 nm ultrabright NPs.[51] Importantly, the cell experiments revealed practically no signal for A20-functionalized PEMA-based NPs (Figures 3B and S1). A similar low intracellular signal was observed for the NPs bearing A20 annealed with T20 DNA. Then, we directly compared PEMA-based NPs functionalized with A20 DNA (A20-NPs) and T20 DNA (T20-NPs). A strong intracellular signal was observed in the case of T20-NPs, while the signal from A20-NPs was very weak and could only be detected when the signal in the image was multiplied 5-fold (Figures 3C and S1). Thus, the use of PEMA-based NPs dramatically decreased nonspecific interactions, allowing direct detection of T20-NPs specifically hybridized with poly(A) targets inside the cells. It could be related to the narrower size

https://doi.org/10.1021/acsnano.1c09409
ACS Nano XXXX, XXX, XXX−XXX

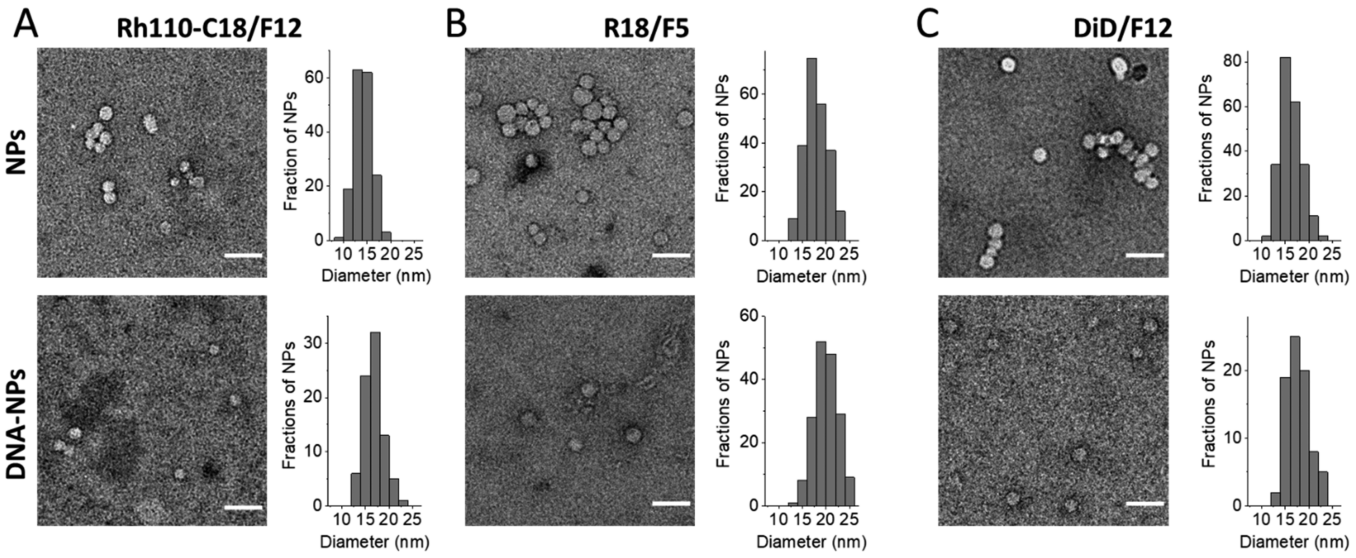

Figure 5. TEM characterization of DNA-NPs of different color functionalized with T20 oligonucleotides. TEM images of DNA-NPs loaded at 30 wt % with Rh110-18/F12 (A), R18/R5-TPB (B), and DiD/F12 (C) and corresponding size distribution histograms at the right (at least 200 NPs were analyzed per condition). Upper panels correspond to bare NPs, while lower panels correspond to DNA-NPs.

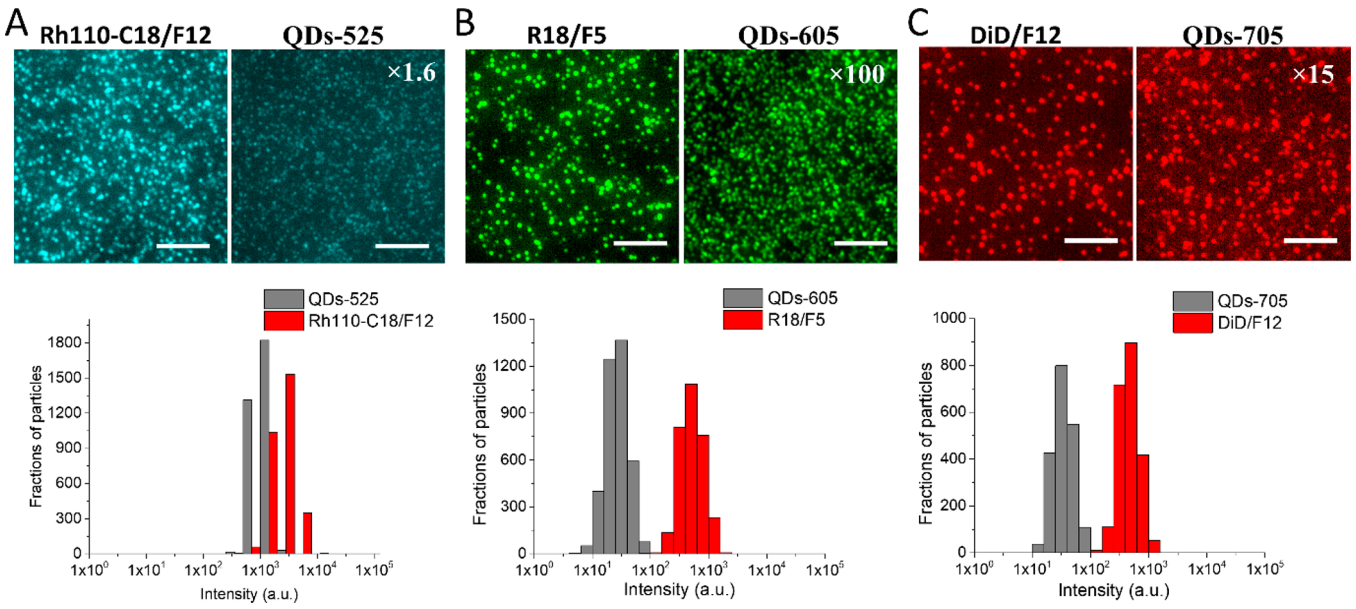

Figure 6. Single-particle characterization of DNA-NPs bearing T20 oligonucleotide in comparison to corresponding QDs on a glass surface using epi-fluorescence microscopy. Upper panels: Fluorescence images of DNA-NPs loaded at 30 wt % with Rh110-C18/F12 *vs* QDs-525 (A), R18/R5-TPB *vs* QDs-605 (B), and DiD/F12 *vs* QDs-705. The signal in QDs was multiplied 1.6- (A) 100- (B), and 15-fold (C) by a corresponding increase in the source power for better comparison with brighter DNA-NPs. Scale bar: 5 μm. Lower panels: Corresponding intensity distribution histograms for DNA-NPs *vs* QDs.

distribution of these PEMA-based NPs (see below) compared to PMMA NPs. The second reason could be the more hydrophobic nature of PEMA compared to PMMA (ethyl *vs* methyl group), which can provide better stability to DNA-NPs, where the core is formed essentially due to hydrophobic collapse of the polymer. It should be added that the small size of PEMA-based NPs should limit the number of grafted oligonucleotides per particle to ~80, according to our earlier studies on analogous DNA-NPs,[51] which is important to minimize the off-target nonspecific interactions.

Then, we functionalized PEMA-based NPs with capture DNA sequences complementary to survivin and β-actin mRNA and tested them in cells. Both nanoprobes showed significant intracellular signal inside the cells (Figures 3D,E and S2), which was significantly higher in the case of β-actin (see below). To verify the contribution of nonspecific interactions, we annealed our DNA-NPs with complementary short oligonucleotides in solution to block their capacity to hybridize with corresponding intracellular mRNA targets. Importantly, the intracellular signal decreased drastically for the double-stranded nanoprobes, so that 5-fold multiplication of the signal was required to observe some cell fluorescence (Figures 3D,E and S2). These first experiments showed that we could observe sequence-specific hybridization of our DNA-NPs with the intracellular mRNA targets. It should be noted that in all these images the nucleus

https://doi.org/10.1021/acsnano.1c09409
ACS Nano XXXX, XXX, XXX−XXX

remained dark, indicating that NPs could not penetrate through the nuclear envelope.

DNA-NPs of Different Color. Next, we prepared NPs of three different colors in order to perform multicolor detection of target mRNA. In addition to red-emitting R18/F5, we selected a green rhodamine 110 derivative with an octadecyl chain (Rh110-C18)[83] and far-red cyanine DiD (Figure 4). As a counterion for these two dyes, we used the bulkiest available counterion F12, which was shown previously to ensure the highest fluorescence quantum yields (QYs) for the NPs.[81,83] We formulated bare NPs loaded with corresponding dyes and checked the QYs at different dye loading. For all three dyes, QYs decreased with an increase in the high loading (Table S1), indicating some effect of dye self-quenching. On the basis of these data, we could choose optimal high loading, where QYs remained significantly high: 30 wt % for all three dye salts, with quantum yields of 52%, 34%, and 42% for R18/F5, R110-C18/F12, and DiD/F12. The size of the obtained bare NPs at 30 wt % dye loading remained small according to dynamic light scattering (DLS) (~17 nm) and TEM (14−18 nm, Table S2). TEM imaging confirmed the spherical shape of bare NPs (Figure 5). Then, we functionalized them with A20 or T20, using the same protocol based on the SPAAC reaction. The QY values did not change after functionalization and thus remained relatively high. The absorption and fluorescence spectra of DNA-NPs showed well-defined and well-separated bands (Figure 4), typical for the molecular forms of these three dyes. These bands match well common optical settings of the microscope in the green, red, and far-red channels. According to the TEM of DNA-NPs, the size of the spherically shaped particles did not significantly change, since only a ~2 nm increase was observed after functionalization (Figure 5, Table S2). It is important to note the relatively narrow size distribution of all these DNA-NPs, so that all detected NPs were systematically <25 nm. This is a key difference with PMMA-based NPs, where for similar particle size, NPs > 30 nm were still observed (Figure 2C). This narrower size distribution could explain why PEMA-based NPs showed much less nonspecific interactions (or NP trapping) inside the cells (see above, Figure 3). On the other hand, DLS data suggested that after DNA functionalization, the particle size increased by 6−7 nm (Table S2), which corresponds to the lengths of two 20mer strands grafted to the NP surface. In contrast to TEM, DLS records the hydrodynamic diameter that takes into account the relatively thick hydration shell formed by grafted nucleic acids.

Then, we characterized the obtained DNA-NPs at the single-particle level using wide-field fluorescence microscopy. For each color of NPs, we made a comparison with corresponding QDs characterized by similar emission wavelength. All studied DNA-NPs, which appeared as dots in the microscopy images, were significantly brighter than corresponding QDs (Figure 6). Quantitative analysis of the single-particle brightness revealed that green, red, and far-red DNA-NPs were 2.3 ± 0.8-, 97 ± 6-, and 16 ± 2-fold brighter than corresponding QDs (Figure 6). These differences correspond to the theoretical brightness (B) of our NPs, which can be expressed as $B = N \times \varepsilon \times QY/100$, where N is the number of dyes per NP, ε is the absorption coefficient (M^{-1} cm^{-1}) at the excitation wavelength used, and QY is the fluorescence quantum yield (%) of the dye inside the NP. Taking the average NP size of bare NPs loaded with Rh110-18/F12, R18/R5-TPB, and DiD/F12 NPs of 14, 18, and 16 nm, respectively, according to TEM, and 30 wt % loading of the dyes *vs* polymer (*i.e.*, 23% *vs* total particle mass), the corresponding estimated N is 85, 308, and 113. Then, the estimated single-particle brightness is 6.9×10^5, 1.8×10^7, and 9.7×10^6 $M^{-1} \times cm^{-1}$ for Rh110-18/F12, R18/R5-TPB, and DiD/F12 NPs. For QDs-525, QDs-605, and QDs-705, the measured QY values were 77%, 52%, and 49%, respectively. Therefore, their corresponding estimated brightness was 1.3×10^5, 3.0×10^5, and 4.4×10^5 M^{-1} cm^{-1} for excitation at 470, 550, and 640 nm, respectively. Thus, theoretically, Rh110-18/F12, R18/R5-TPB, and DiD/F12 should be 5.3-, 60-, and 22-fold brighter than QDs-525, QDs-605, and QDs-705, respectively, which is close to the obtained experimental values. We should note that these differences would be smaller if QDs were excited at the violet region, where their absorption coefficient is higher. The green DNA-NPs were significantly less bright than the other two DNA-NPs because of a lower absorption coefficient at the excitation wavelength used (470 nm of LED), lower QY of this dye, and less optimal emission filter settings. Overall, we obtained DNA-NPs of similar small size and high brightness, which can be used for multicolor RNA-FISH experiments.

Multicolor Detection of mRNA. We functionalized NPs of three different colors with three capture sequences targeting poly(A), β-actin, and survivin fragments of mRNA. After incubation of DNA-NPs with fixed and permeabilized HeLa cells, we observed corresponding staining in each channel: green for β-actin, red for survivin, and blue for poly(A) targets (Figure 7). Then, to verify that the binding is sequence dependent, we annealed each nanoprobe with a corresponding complementary DNA oligonucleotide and tested in cells. The obtained double-stranded DNA-NPs showed practically no emission inside cells, which confirmed low nonspecific interactions between NPs and cells. To provide a more direct control for the sequence

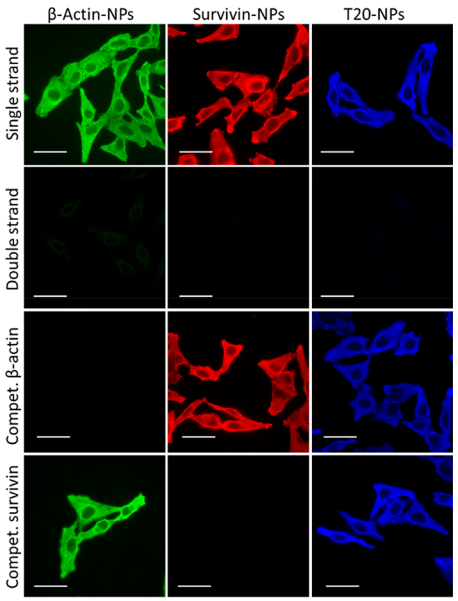

Figure 7. Validation of DNA-NPs for detection of intracellular mRNA targets in fixed HeLa cells. Single-stranded probes β-actin-NPs loaded with Rh110-C18/F12, survivin-NPs loaded wth R18/F5, and A20-NPs loaded with DiD/F12 for β-actin, survivin, and poly(A) sequences of mRNA were compared to controls with double-stranded DNA-NPs (annealed with complementary sequences) and competitor oligonucleotides (100 nM) for corresponding β-actin and survivin sequences added 1 h before addition of DNA NPs. DNA-NPs concentration expressed in encapsulated dyes was 100 nM. Scale bar: 50 μm.

https://doi.org/10.1021/acsnano.1c09409
ACS Nano XXXX, XXX, XXX−XXX

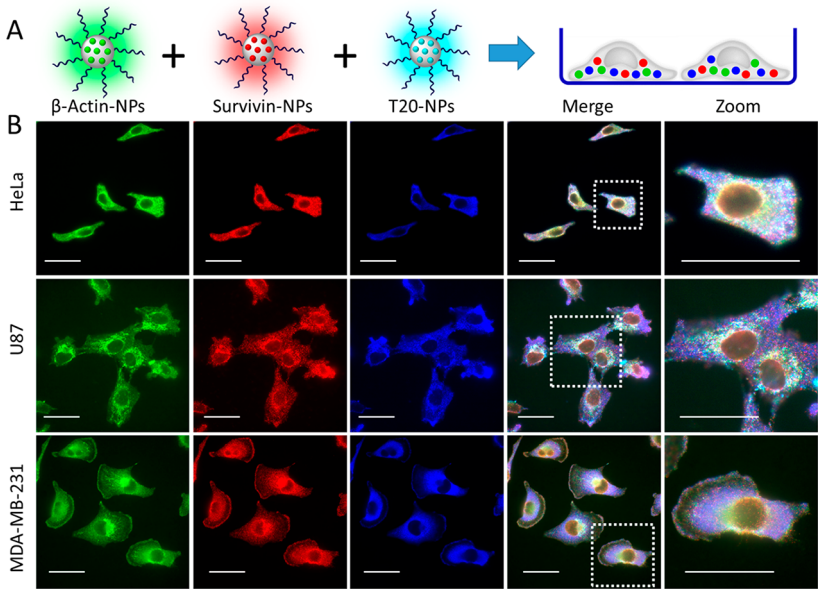

Figure 8. Multiplexed detection of mRNA sequences in fixed cells by AmpliFISH. (A) General principle and (B) corresponding epi-fluorescence images of three nanoprobes (the same as in Figure 7) β-actin-NPs (green), survivin-NPs (red), and T20-NPs (blue) in three cell lines: HeLa (upper row), U87 (middle row), and MDA-MB-231 (lower row). Merging of three channels and corresponding zoomed-in images of cells are also shown (last two columns). A mixture of the three different NPs at 100 nM (total dye concentration) was added to cells during 1 h, then washed two times before the observations. Scale bar: 50 μm.

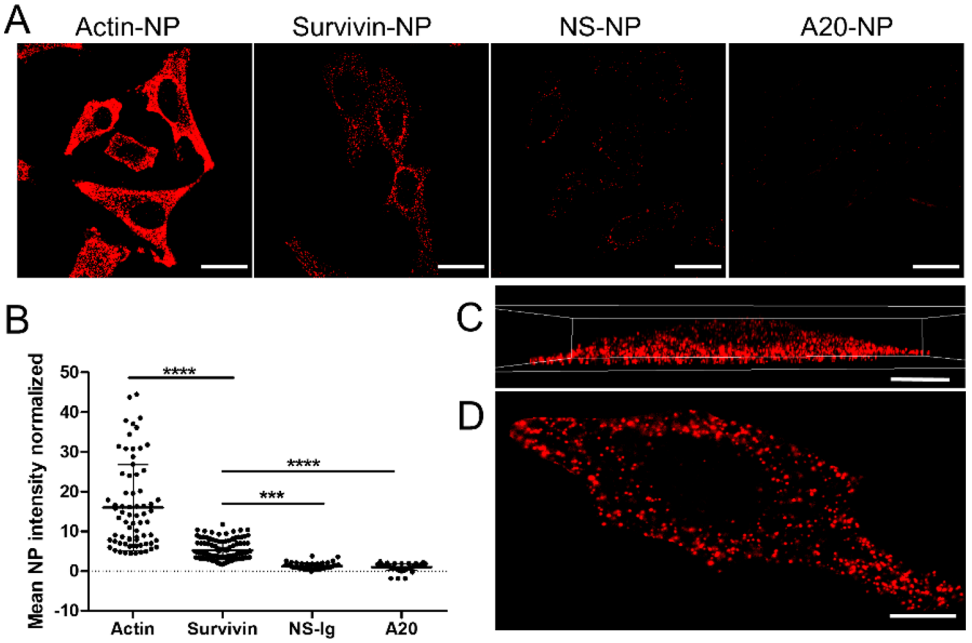

Figure 9. Imaging of HeLa cells using AmpliFISH with spinning-disk microscopy and quantification of the signal from mRNA targets. (A) Z-projection of multiple images of HeLa cells stained with different DNA-NPs. Scale bar: 30 μm. (B) Quantification of total fluorescence intensity from DNA-NPs for four different target mRNA sequences. At least 100 cells were analyzed per condition in three independent measurements. ***$p < 0.001$, ****$p < 0.0001$. (C) 3D reconstruction of HeLa cells labeled with survivin-NPs. (D) Selected $X-Y$ plane of the same cell as in (C) obtained by spinning-disk microscopy. Scale bar (C, D): 12 μm.

specificity of our FISH probes, we treated the fixed and permeabilized cells with a competitive sequence complementary to the target (*i.e.*, identical to the capture sequence grafted to NPs), which is expected to block the site of binding of our nanoprobes. Importantly, the β-actin competitor turned off the intracellular signal from nanoprobes for β-actin, but did not influence those for survivin or poly(A) (Figure 7). By contrast, a competitive sequence encoding survivin blocked binding of survivin nanoprobes, but did not affect those targeting actin or poly(A). These experiments showed that our NPs bind intracellular targets with sequence specificity for NPs of different color. We repeated these experiments for U87 (Figure S3) and MDA-MB-231 (Figure S4) cells and obtained similar results with excellent inhibition for both double-stranded version of NPs and the competitors for the β-actin and survivin mRNA targets. Thus, the approach works for multiple cell lines.

https://doi.org/10.1021/acsnano.1c09409
ACS Nano XXXX, XXX, XXX−XXX

The next challenge was to image all three target sequences simultaneously by exploiting three colors of NPs bearing corresponding targeting oligonucleotides. To this end, fixed and permeabilized HeLa, U87, and MDA-MB-231 cells were incubated simultaneously with three NPs of different color and further imaged using three channels of the microscope (Figure 8). Importantly, we could obtain signals for all three nanoprobes within the same cell. Each cell showed a distinctive combination of three colors distributed in space (Figure 8B). The green and red colors, encoding β-actin-NPs and survivin-NPs, respectively, did not really colocalize, which can be seen in the zoomed images. This observation was confirmed by a Manders' colocalization, giving relatively low values for β-actin-NPs in survivin-NPs and *vice versa* for all three cell lines (with only one exception for MDA-MB-231, Table S3). On the other hand, each of them colocalized with the poly(A) target, which can be seen from dominating magenta and cyan colors of the cells (Figure 8B). Indeed, high Manders' colocalization coefficients for β-actin-NPs in T20-NPs were observed, namely, 0.998, 0.998, and 0.935 for HeLa, U87, and MDA-MB-231, respectively (Table S3). Similar high values were observed for survivin. These observations can be explained by the fact that both β-actin and survivin mRNAs are expected to have poly(A). On the other hand, T20-NPs colocalized with much lower Manders' coefficients with β-actin-NPs and survivin-NPs, which is normal because there are many other mRNAs having a poly(A) tail. In the perinuclear regions, all three colors appeared colocalized, giving white pixels. The latter is probably because too many particles of different color concentrated within areas below the diffraction-limited resolution of the microscope, which produced a colocalization effect, even if these NPs are not bound to the same mRNA target. One could also notice that the distribution of the three colors was slightly different for each studied cell line. Indeed, HeLa cells showed a tendency to redistribute colors in a rather homogeneous fashion, while the U87 cells showed magenta colors (*i.e.*, survivin and poly(A)) localized at extremities of the cells (Figure 8B). In MDA-MB-231 cells, the signals corresponding to β-actin and survivin appeared in similar areas, including the cell edges, providing characteristic yellow regions (Figure 8B). Thus, the combination of three nanoprobes reveals distinctive signatures of mRNA distribution at the single-cell level for each cancer cell line.

Quantification and Single-Particle Analysis. We explored a possibility to quantify the observed fluorescence inside the HeLa cells with different DNA-NPs loaded with the same dye, R18/F5. In addition to β-actin, survivin, and A20, we prepared nanoprobes functionalized with another noncoding capture sequence (NP-NS) that does not correspond to any mRNA in HeLa cells. Using spinning-disk fluorescence microscopy, we recorded different planes of the cells and then summed all stacks together. The resulting images could clearly show the strong signal from β-actin-NPs, then a lower signal from survivin-NPs and practically no signal from noncoding sequence NS-NPs and A20-NPs (Figure 9A). Quantitative analysis confirmed these observations, showing that the average signal decreased in the following order: β-actin-NP $\gg$ survivin-NP $\gg$ NS-NP > A20-NP (Figure 9B). RT-qPCR of the cells revealed that mRNA of β-actin was much more abundant (Ct = 15.2) than that of survivin (Ct = 24.8), supporting our FISH data. However, the differences revealed by RT-qPCR were significantly larger than those observed by the AmpliFISH method. Therefore, we consider that our approach at this step remains semiquantitative. One should also note that NS-NPs showed a bit higher signal than A20-NPs, which indicates that a part of the signal here could originate from off-target interactions of the noncoding sequence. Taking into account that the presence of a competitive sequence can completely block the binding of corresponding DNA-NPs, we can conclude that nonspecific binding of NPs could be related to some off-target hybridization with shorter nucleic acid sequences, which is a common problem of the FISH technique.[41,88] This could explain why at the current state our method remains semiquantitative.

The remaining question regarding our DNA-NPs in cells was whether the observed spots correspond to individual NPs. In the wide-field microscopy images (Figures 7 and 8), it was difficult to identify single particles because of poor Z-resolution and strong contribution of out-of-focus NPs to the final images. Therefore, we used spinning-disk microscopy to record the Z-stack of image planes of cells labeled with survivin-NPs and then reconstructed 3D images. In the 3D image (Figure 9C, Video S1) and the individual XY image plane (Figure 9D), one could clearly see individual dots distributed all around the cells, except the nucleus, where NPs cannot really penetrate. In addition, we recorded videos from one focal plane of HeLa cells labeled with actin-NPs using spinning-disk microscopy. We found that the majority of bright dots (with the exception of some larger spots) showed some signal fluctuation/blinking (Video S2). This fluorescence intermittence is typical for individual acrylate-based R18/F5-loaded NPs due to cooperative effects of dyes inside the polymeric particle.[78] Therefore, we can conclude that these dots correspond to single particles immobilized inside the cells through interactions with the target.

Comparison with the Classical FISH Method. To benchmark the performance of AmpliFISH, a commercial FISH technique was used, employing locked nucleic acid (LNA) probes (Qiagen). The LNA technology provides improved discriminating capacity of FISH probes and thus improved sensitivity and specificity to the RNA targets.[89] Two types of LNA probes were tested: LNA T25 in order to target poly(A) of mRNA and LNA β-actin, which groups together several sequences targeting actin mRNA. These two types of probes are coupled to digoxigenin (3′DIG) to allow indirect detection of mRNA targets (primary antibody then secondary antibody coupled to Alexa Fluor 488). The results obtained for these two probes as well as the negative control (absence of probe) for the U87 line are illustrated in Figure 10. On one hand, there is indeed an absence of fluorescence signal for the negative control without LNA probes, ruling out nonspecific interactions in the cells. On the other hand, a fluorescence signal is obtained for the LNA probes in the fixed and permeabilized U87MG cells, in the cytosol and in the nucleus. Unlike DNA-NPs, these probes are capable of detecting their target in the nucleus, owing to their smaller size. However, the key difference was the obtained signal with the commercial probes was 8 times lower compared to that obtained with our green emission DNA-NPs loaded with Rh110-18/F12. Taking into account that our red NPs loaded with R18/F5 are 25 times brighter than the green ones (see above), our AmpliFISH technique based on R18/F5 should provide a 200-fold stronger signal compared to the LNA FISH method. This drastic difference originates from the much higher brightness of our NPs (80−300 dyes per NP) compared to the fluorescently labeled antibodies. In addition, our technique is much simpler and faster compared to the commercial FISH composed of >20 steps before microscopy accompanied by multiple washes between each step.

https://doi.org/10.1021/acsnano.1c09409
ACS Nano XXXX, XXX, XXX−XXX

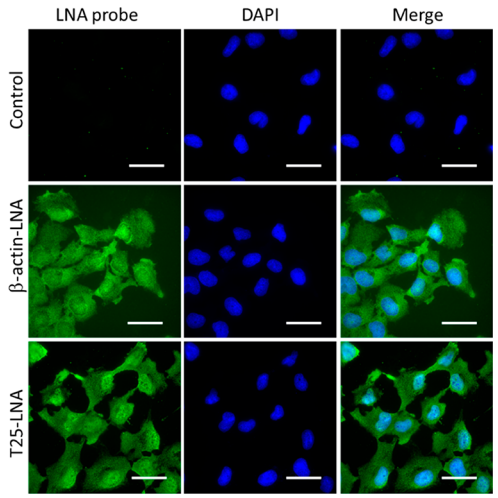

Figure 10. Commercial LNA probes at 25 nM for the detection of actin mRNA and poly(A) tails in U87 cells. Epi-fluorescence images of the FISH LNA probes and nuclei (DAPI) as well as the superposition (merge) of the two images (scale bar: 50 μm).

CONCLUSIONS

The development of simple and direct methods for the detection of mRNA inside the cells, which could accelerate biological and biomedical research and clinical diagnostics, remains a high challenge. To address this problem, we propose an amplified FISH methodology (AmpliFISH): ultrabright DNA-functionalized polymeric NPs are specially designed to penetrate cells and detect their intracellular mRNA targets. We synthesized NPs of different sizes and polymeric matrices. We found that the size of NPs below 20 nm is crucial for penetration and mRNA targeting in the fixed and permeabilized cells. Moreover, the nature of the polymer can drastically influence nonspecific interactions, which allowed us to select polymeric NPs showing the highest specificity. The obtained DNA-NPs enable sequence-specific detection and imaging of mRNA encoding β-actin, survivin, and its poly(A) tail, based on a very simple protocol of cell preparation and short incubation with NPs. Moreover, a combination of three different colors enables simultaneous detection of three mRNA targets within the same cell, showing feasibility of simple multiplexing single-cell transcriptome analysis. Importantly, each cancer cell line displayed a characteristic intracellular distribution of the three mRNA sequences, like a cell fingerprint. Moreover, the method allows semiquantitative analysis of mRNA in cells, although an additional dedicated study will be required to make it a truly quantitative single-cell mRNA detection method. Single-particle video microscopy confirmed that the majority of the intracellular signal corresponds to individual particles, which should enable mRNA detection with single-molecule sensitivity. Comparison with the commercial FISH technique based on LNA oligonucleotides showed that our method has multiple advantages: (i) it provides 8−200-fold stronger signal (dependent on the NP color); (ii) it is based on three steps *vs* ~20 steps in the commercial technique as well as much shorter time. Thus, the developed AmpliFISH approach has the potential to significantly improve the current methods of transcriptomic analysis at the single-cell level, which is important for both biological research and clinical diagnostics.

MATERIALS AND METHODS

Chemical Synthesis. Chemicals were purchased from either Sigma-Aldrich, Alfa Aesar, or ThermoFisher Scientific. NMR spectra were recorded at 20 °C on a Bruker Avance III 400 MHz spectrometer, and chemical shifts were reported as delta scale in ppm relative to $CHCl_3$ (δ = 7.26 ppm) for ^{1}H NMR and $CDCl_3$ (δ = 77.16 ppm) for ^{13}C NMR. Mass spectra were obtained using an Agilent Q-TOF 6520 mass spectrometer. Polymers PMMA-AspN3-1.6%, PMMA-AspN3-5%, and PEMA-AspN3 were synthesized as described previously[51,52] Rhodamine B octadecyl ester trakis(pentafluorophenyl)borate (R18/F5) and DiD/F12 were synthesized by ion exchange and purified by column chromatography as described previously.[77,81] Rhodamine 110 octadecyl ester (Rh110-C18/Cl) was synthesized by coupling of rhodamine 110 chloride and 1-octadecanol in the presence of sulfuric acid, followed by column chromatography purification as described elsewhere.[90] Rhodamine 110 octadecyl ester tetrakis[3,5-bis-(1,1,1,3,3,3-hexafluoro-2-methoxy-2-propyl)phenyl]borate trihydrate (Rh110-C18/F12) was obtained by the ion exchange of obtained Rh110-C18/Cl with a sodium tetrakis[3,5-bis(1,1,1,3,3,3-hexafluoro-2-methoxy-2-propyl)phenyl]borate trihydrate (F12) followed by purification on preparative TLC using dichloromethane/methanol 95/5 as eluent.

Preparation of NPs. Sodium phosphate monobasic (>99.0%, Sigma-Aldrich) and sodium phosphate dibasic dihydrate (>99.0%, Sigma- Aldrich) were used to prepare 20 mM phosphate buffers. Sodium tetraborate decahydrate (>99.0%, Sigma-Aldrich) was used to prepare borate buffer. The final pH was adjusted with 0.1 M hydrochloride acid or 0.1 M sodium hydroxide. Milli-Q water (Millipore) was used in all experiments.

NP-PMMA-MA-1.6%. A 100 μL amount of the polymer solution in acetonitrile (2 mg mL^{-1} with 30 wt % of R18/F5 relative to the polymer) was added quickly using a micropipet to 900 μL of 20 mM phosphate buffer, pH 7.4, under shaking (Thermomixer comfort, Eppendorf, 1100 rpm). Then, the residues of acetonitrile were evaporated.

NP-PMMA-MA-5% and NP-PEMA-MA (Multicolor). A 50 μL amount of the polymer solution in acetonitrile (2 mg mL^{-1} containing Rh110-C18/F12 at 30 wt %, R18/F5 at 50 wt %, or DiD/F12 at 30 wt % relative to the polymer) was added quickly using a micropipet to 450 μL of 10 mM borate buffer, pH 9, at 21 °C under shaking (Thermomixer comfort, Eppendorf, 1100 rpm). While continuing mixing, 500 μL of 20 mM phosphate buffer, pH 6, was added. Then, the residues of acetonitrile were evaporated. The particle solution was then diluted 2-fold with the 20 mM phosphate buffer, pH 7.4.

General Protocol for Functionalization of NPs with DNA. Lyophilized single-strand DNA sequences were purchased from IBA GmbH, dissolved in Milli-Q water, aliquoted, and stored at −20 °C for further experiments. Aliquots of corresponding DNA-DBCO (concentration of 60 μM in the reaction mixture) were added to 200 μL of corresponding nanoparticles. The reaction was mixed and kept overnight at 40 °C without shaking protected from light. Then the reaction was cooled to room temperature. In the case of NPs with a double strand, to 100 μL of the reaction mixture an aliquot of DNA-target sequence in a 1:1 ratio with DNA-DBCO was added and the mixture was heated to 70 °C in a water bath for 3 min. To complete hybridization, the reaction was cooled to room temperature and kept in the dark for 2 h. Then, in the case of single-strand nanoparticles the mixture was diluted with 20 mM phosphate buffer to 4 mL. In the case of the double-strand nanoparticles, the mixture was diluted with 20 mM phosphate buffer containing 12 mM $MgCl_2$ and 30 mM NaCl to 4 mL. Both types of NPs were purified by centrifugation using centrifuge filters (Amicon, 0.5 mL, 100 kDa, Sigma-Aldrich) at 1000*g* at 20 °C for 2 min. The procedure of centrifugation was repeated five times to remove the nonreacted oligonucleotides using the corresponding buffer. The obtained functionalized DNA-NPs were kept in the dark at 4 °C.

The oligonucleotide sequences used in this study are shown below:

SurC-DBCO, 5′-CCC AGC CTT CCA GCT CCT TGA-(DBCO)-3′

https://doi.org/10.1021/acsnano.1c09409
ACS Nano XXXX, XXX, XXX−XXX

SurC-Target, 5′-CAA GGA GCT GGA AGG CTG GG-3′
SurC-Competitive, 5′-CCC AGC CTT CCA GCT CCT TGA-3′
Actin-DBCO, 5′-CTG ACC CAT GCC CAC CAT CA-(DBCO)-3′
Actin-Target, 5′-TGA TGG TGG GCA TGG GTC AG-3′
Actin-Competitive, 5′-CTG ACC CAT GCC CAC CAT CA-3′
T20-DBCO, 5′-TT TTT TTT TTT TTT TTT TT-(DBCO)-3′
T20, 5′-TT TTT TTT TTT TTT TTT TT-3′
A20-DBCO, 5′-AAA AAA AAA AAA AAA AAA AA-(DBCO)-3′

Characterization of NPs. Dynamic light scattering (DLS) measurements were performed on a Zetasizer Nano ZSP (Malvern Instruments S.A.). The Zetasizer software provided with standard cumulates and size distribution by volume analysis was used to characterize nanoparticles by DLS. For the data analysis, the following parameters were used: for the solvent (water), temperature 25 °C, refractive index RI 1.33, and viscosity 0.8872 cP. Nanoparticles were assumed to be all homogeneous and spherical in shape. Absorption spectra were recorded on a Cary 5000 scan UV−visible spectrophotometer (Varian). Excitation, emission spectra, and anisotropy were recorded on a FS5 spectrofluorometer (Edinburg Instruments). For standard recording of fluorescence spectra, the excitation wavelength was set to 470 nm (Rh110-C18/F12), 530 nm (R18/F5), and 640 nm (DiD/F12). The fluorescence spectra were corrected for detector response and lamp fluctuations. Quantum yields of NPs and QDots were calculated using fluorescein in 10 mM NaOH (QY = 1.0), rhodamine 101 in methanol (QY = 1.0),[91] and DiD in methanol (QY = 0.33)[92] as the corresponding references.

Transmission Electron Microscopy. Carbon-coated copper−rhodium electron microscopy grids with a 300 mesh (Euromedex, France) were surface treated with a glow discharge in amylamine atmosphere (0.45 mbar, 5−5.3 mA, 25 s) in an Elmo glow discharge system (Cordouan Technologies, France). Then, 5 μL of the solution of NPs was deposited onto the grids and left for 2 min. The grids were then treated for 1 min with a 2% uranyl acetate solution for staining. They were observed with the Tecnai F20 electron microscope, equipped with a FEG operated at 200 keV. Areas covered with nanoparticles of interest were recorded at 29000× magnifications on a GATAN CCD 2K*2K "US10001" camera. Image analysis was performed using the Fiji software.

Single-Particle Fluorescence Microscopy. Immobilization of DNA-NPs and QDots was done as follows. The LabTek chamber (borosilicate cover glass, eight wells, ThermoFisher Scientific) was washed three times with PBS followed by incubation with 200 μL of bovine serum albumin (BSA)−biotin (Sigma-Aldrich) 0.5 mg mL^{-1} in PBS for 5 min. Then, the BSA−biotin solution was removed, and the chamber was washed three times with 500 μL of PBS. In the case of nanoparticle immobilization, the chamber was incubated with 200 μL of neutravidin (ThermoFisher Scientific) solution (0.5 mg mL^{-1} in PBS) for 5 min and washed three times with 500 μL of PBS. Then the chamber was incubated with 200 μL of a 1 μM solution of A20-biotin in PBS for 5 min and washed one time with PBS and two times with 20 mM phosphate buffer. Then the nanoprobe solution was deposited with proper concentration to achieve the desired density and incubated for 1 h at room temperature in the dark. Before measurements the chamber was washed two times with 20 mM phosphate buffer and covered with 200 μL of the same buffer. In the case of QDot immobilization, QDot525 streptavidin conjugate, QDot605 streptavidin conjugate, and QDot705 streptavidin conjugate (ThermoFisher Scientific) were diluted to 10 pM final concentration in PBS, and 300 μL was added to the chamber. After 1 h of incubation, the chamber was washed three times with 500 μL and filled with 200 μL of PBS.

Single-particle microscopy measurements were performed in the epi-fluorescence mode using a Nikon Ti-E inverted microscope with a 100× objective (Apo TIRF, oil, NA 1.49, Nikon). The excitation was provided by light-emitting diodes (SpectraX, Lumencor) with the following wavelength and power density: 470 nm at 14 and 23 W cm^{-2} for Rh110-C18/F12 NPs and QDot525, respectively; 550 nm at 0.24 and 24 W cm^{-2} for R18/F5 NPs and QDot605, respectively, and 640 nm at 1.1 and 17 W cm^{-2} for DiD/F12 NPs and QDot705. The exposure time was set to 400 ms per image frame. The fluorescence signal was recorded with a Hamamatsu Orca Flash 4 camera.

Single-particle analysis was performed using the Fiji software. Particle locations were detected through a Fiji routine applied to a projection (maximum intensity) of all obtained frames per experiment. After the automatic background subtraction, the mean intensities of circular regions of interest with a diameter of 8 pixels around the found particle locations were then measured. At least three image sequences (245 pixel × 245 pixel) per condition with, on average, 1000−2000 particles per sample were analyzed.

Cell Culture. HeLa cells (ATCC CCL-2) were grown in Dulbecco's modified Eagle's medium low glucose (DMEM, Gibco), supplemented with 10% fetal bovine serum (FBS, Dutscher), 1% L-glutamine (Lonza), and 1% penicillin−streptomycin (Lonza). The human glioblastoma cell line U87 (ATCC) was maintained in minimum essential medium (MEM, Gibco) supplemented with 10% FBS, 1% L-glutamine, 1% sodium pyruvate (Lonza), and 1% nonessential amino acid (Lonza). The human breast cancer cell line MDA-MB-231 (ATCC) was grown in MEM (Gibco) supplemented with 10% FBS and 1% ultraglutamine (Lonza). All cell lines were maintained at 37 °C in a humidified atmosphere containing 5% CO_2. For the different experiments, cells were seeded in eight-well LabTek plates (ThermoFisher) at 8000 cells/well overnight.

Cell Fixation and Permeabilization. For the fixation step, a standard protocol of immunofluorescence was applied. First, cells were washed one time with Dulbecco's phosphate-buffered saline (DPBS, Lonza) and incubated with 4% PFA during 12 min at 37 °C. Cells were then washed two times with DPBS and incubated 1 min at RT with 0.1% Triton X-100. Then, cells were washed two times with DPBS and incubated in 3% BSA/DPBS (Sigma) for 1 h 30 min at RT. The final step was to remove the 3% BSA/DPBS solution and incubate cells in DPBS. The fixed cells can be used just after fixation or can be kept at 4 °C until their utilization.

***In Situ* Hybridization with DNA-NPs.** Independently of the DNA sequence used, DNA-NPs were first diluted to 100 nM concentration in 0.1% BSA/DPBS. Then, DPBS from the fixed permeabilized cells was removed and the diluted DNA-NPs were added to the cells for 1 h at RT or 37 °C. Then, cells were washed two times with 0.1% BSA/DPBS to remove the DNA-NPs that were not hybridized with the RNA target and were observed by the microscope in 0.1% BSA/DPBS.

In the case of competition experiments, cells were preincubated for 1 h at RT with a complementary DNA sequence to actin or survivin mRNA target at 100 nM diluted in 0.1% BSA/DPBS. Without any washing step, NPs were directly added on cells, followed by the above-described protocol.

Cell Imaging. At the beginning of the study, cells and NPs were observed at TIRF mode using a Nikon Ti-E inverted microscope with a 100× objective (Apo TIRF, oil, NA 1.49, Nikon). The excitation wavelength was 550 nm with a power density of 26 W cm^{-2}; emission was recorded with a 600/50 nm band-pass filter. Then, images were acquired in epi-fluorescence mode with a Nikon Ti-E inverted microscope, with a 60× oil objective (NA 1.4, Nikon) and a Hamamatsu Orca Flash 4 sCMOS camera. The excitation was provided by light-emitting diodes (LED, SpectraX, Lumencor). Acquisition settings were as follows: for Rh110-C18/F12 NPs (ex. 470 nm; emission: 531/40 nm band-pass filter) with an excitation power density of 5 W cm^{-2} and exposure time of 300 ms, for R18/F5 NPs (ex. 550 nm; emission: 600/50 nm band-pass filter) with an excitation power density of 3 W cm^{-2} and exposure time of 200 ms, and for DiD/F12 NPs (ex. 638 nm; emission: 705/72 nm band-pass filter) with an excitation power density of 1.3 W cm^{-2} and exposure time of 200 ms. The images were recorded using NIS Elements and then processed with ImageJ software. Colocalization analysis was performed using Manders' coefficient with the JACoP plugin in Fiji software. A threshold was applied for each channel of all images (1685 to actin, 1613 to survivin, and 1531 to T20).

Quantitative cellular imaging with R18/F5 NPs (Figure 9) was performed using a Nikon Ti-E inverted microscope, equipped with a CFI Plan Apo 60× oil (NA = 1.4) objective, X-Light spinning-disk module (CREST Optics), and a Hamamatsu Orca Flash 4 sCMOS camera with a 600/50 nm band-pass filter. The excitation in confocal mode was provided by a 532 nm diode laser (OXXIUS). The exposure

https://doi.org/10.1021/acsnano.1c09409
ACS Nano XXXX, XXX, XXX−XXX

time in confocal mode was set to 500 ms per image frame. All the images were recorded using NIS Elements and then processed using Fiji software. Background was removed in all images using a filter rolling ball with a 20 pixels' radius and a sliding paraboloid shape. All images are presented with the same brightness and contrast. Mean fluorescence intensity was measured on the 3D stack for around 100 cells per condition from three independents experiments. Statistical analysis was done with the ANOVA algorithm.

RT-qPCR. Cell line selection was based on surviving mRNA expression. Two days before RNA extraction, 10^6 cells were seeded in 100 mm Petri dishes. Total RNA was isolated using a miRNeasy mini kit (Qiagen) following the protocol provided by the manufacturer. The final volume of elution was 40 μL. The quantity of total RNA was determined using a Nanodrop (Thermo Scientific). RNA samples were aliquoted and stored at −80 °C. Then, 1 μg of RNA extracted was transcribed into cDNA using miScript II reverse transcription kit (Qiagen). mRNA expression was evaluated by relative quantitative RT-qPCR analysis using the Fast SYBR Green Master Mix PCR kit (Qiagen) and the StepOne Plus real time PCR system (Applied Biosystem), according to the manufacturer's protocol. The primers used were β-actin (RT^2qPCR Primer Assay for Human ACTB, NM_001101, Qiagen) and BIRC5 (RT^2qPCR Primer Assay for HumanNM_001168, Qiagen). RT-PCR was carried out with human RNA 18S (5′-TGTGGTGTTGAGGAAAGCAG-3′ and 5′-TCCAG ACCATTGGCTAGGAC-3′, Invitrogen) as internal reference. Target cDNA expression was quantified using the comparative ΔΔCt method with 18S rRNA as an internal control.

FISH with Commercial LNA Probe. To compare our results with commercial *in situ* hybridization, poly(T)25 and β-actin LNA probes (Qiagen) were used coupled with DIG as described in the manufacturer's protocol (Exiqon). The DIG proteins were detected thanks to an indirect method, in order to amplify the signal with anti-DIG primary antibody and secondary antibody coupled with fluorochromes. Briefly, the first day, U87MG cells were seeded on 22 mm diameter coverslips deposited on six-well plates and allowed to rest overnight. Then, cells were washed once with DPBS and fixed with 4% PFA (Thermo Scientific)/5% acetic acid (Sigma) in DPBS for 15 min. U87 cells were washed 2 × 5 min in DPBS, treat with pepsin (Merck) (0.1% in 10 mM HCl) for 1 min at 37 °C, and washed again two times with water. At this step, cells were dehydrated through 70%, 90%, and 100% ethanol and allowed to dry a few seconds. Then, 25 μL probes diluted at 25 nM in hybridization buffer (50% deionized formamide (Merck), 2× SSC (ThermoFisher), 50 mM sodium phosphate (Merck), 10% dextran sulfate (Merck)) were put on a slide and covered with the coverslips. The montage was heated at 80 °C for 75 s, and the hybridization step was performed for 30 min in a humid chamber at 55 °C for poly(T)25 probes and at 62 °C for β-actin probes. Then, coverslips were washed with 2× SSC containing 0.1% Tween 20 and washed 3 × 5 min with 0.1× SSC at 65 °C. Cells were dehydrated through 70%, 90%, and 100% ethanol and allowed to dry a few seconds. Finally, U87MG cells were incubated with 3% BSA/DPBS (Sigma) for 1 h 30 min at RT, followed by the anti-DIG grom mouse IgG primary antibody (Sigma) at 1 μg/mL in 3% BSA/DPBS overnight at 4 °C in a humid chamber. The day after, cells were washed 3 × 5 min in DPBS and incubated with goat anti-mouse IgG secondary antibody coupled with Alexa Fluor 488 nm (ThermoFisher) diluted at 1 μg/mL and DAPI (ThermoFisher) diluted at 5 μg/mL for 45 min. After 3 × 5 min of washing with DPBS, cells were mounted on a microscope slide with mounting medium (Dako) and allowed to dry in the dark overnight. Finally, coverslips were observed with epi-fluorescence mode with a Nikon Ti-E inverted microscope, with a 60× oil objective (numerical aperture = 1.4) and a Hamamatsu Orca Flash 4 sCMOS camera. The settings were as follows: DAPI (excitation 395 nm; emission 468−552 nm) with a power of 30% and exposure time of 200 ms and Alexa 488 nm (excitation 470 nm; emission 491−571 nm) with a power of 90% and exposure time of 200 ms. The images were recorded using NIS Elements and then processed with ImageJ software.

ASSOCIATED CONTENT

Supporting Information

The Supporting Information is available free of charge at https://pubs.acs.org/doi/10.1021/acsnano.1c09409.

Additional characterization data, cellular images, and colocalization analysis (PDF)

Video of an individual XY image plane (AVI)

Video of signal fluctuation/blinking (AVI)

AUTHOR INFORMATION

Corresponding Author

Andrey S. Klymchenko − *Laboratoire de Bioimagerie et Pathologies, UMR 7021 CNRS, Faculté de Pharmacie, Université de Strasbourg, 67401 Illkirch, France;* orcid.org/0000-0002-2423-830X; Phone: +33 368 85 42 55; Email: andrey.klymchenko@unistra.fr

Authors

Sylvie Egloff − *Laboratoire de Bioimagerie et Pathologies, UMR 7021 CNRS, Faculté de Pharmacie, Université de Strasbourg, 67401 Illkirch, France*

Nina Melnychuk − *Laboratoire de Bioimagerie et Pathologies, UMR 7021 CNRS, Faculté de Pharmacie, Université de Strasbourg, 67401 Illkirch, France*

Elisabete Cruz Da Silva − *Laboratoire de Bioimagerie et Pathologies, UMR 7021 CNRS, Faculté de Pharmacie, Université de Strasbourg, 67401 Illkirch, France;* orcid.org/0000-0003-3417-5661

Andreas Reisch − *Laboratoire de Bioimagerie et Pathologies, UMR 7021 CNRS, Faculté de Pharmacie, Université de Strasbourg, 67401 Illkirch, France*

Sophie Martin − *Laboratoire de Bioimagerie et Pathologies, UMR 7021 CNRS, Faculté de Pharmacie, Université de Strasbourg, 67401 Illkirch, France*

Complete contact information is available at: https://pubs.acs.org/10.1021/acsnano.1c09409

Author Contributions

[§]S.E. and N.M. contributed equally to this work.

Notes

The authors declare the following competing financial interest(s): Nina Melnychuk, Andreas Reisch, and Andrey S. Klymchenko are inventors on a patent application related to this technology (European patent application no. 18305253.9). The remaining authors declare no competing interests.

ACKNOWLEDGMENTS

This work was supported by the European Research Council ERC Consolidator Grant BrightSens 648525, ERC Proof of Concept Grant AmpliFISH 899928, and SATT Conectus Maturation Grant NanoAntenna. We thank Corinne Crucifix from the FRISBI platform for her help with the electron microscopy and Anne Runser for help with polymer synthesis.

REFERENCES

(1) Michelini, F.; Jalihal, A. P.; Francia, S.; Meers, C.; Neeb, Z. T.; Rossiello, F.; Gioia, U.; Aguado, J.; Jones-Weinert, C.; Luke, B.; Biamonti, G.; Nowacki, M.; Storici, F.; Carninci, P.; Walter, N. G.; di Fagagna, F. D. From "Cellular" RNA to "Smart" RNA: Multiple Roles of RNA in Genome Stability and Beyond. *Chem. Rev.* **2018**, *118*, 4365−4403.

(2) Fatica, A.; Bozzoni, I. Long Non-Coding RNAs: New Players in Cell Differentiation and Development. *Nat. Rev. Genet.* **2014**, *15*, 7−21.
(3) Xia, Y. Q.; Zhang, R. L.; Wang, Z. L.; Tian, J.; Chen, X. Y. Recent Advances in High-Performance Fluorescent and Bioluminescent RNA Imaging Probes. *Chem. Soc. Rev.* **2017**, *46*, 2824−2843.
(4) Dean, K. M.; Palmer, A. E. Advances in Fluorescence Labeling Strategies for Dynamic Cellular Imaging. *Nat. Chem. Biol.* **2014**, *10*, 512−523.
(5) Tyagi, S. Imaging Intracellular RNA Distribution and Dynamics in Living Cells. *Nat. Methods* **2009**, *6*, 331−338.
(6) Femino, A. M.; Fay, F. S.; Fogarty, K.; Singer, R. H. Visualization of Single RNA Transcripts *in Situ*. *Science* **1998**, *280*, 585−590.
(7) Saliba, A.-E.; Westermann, A. J.; Gorski, S. A.; Vogel, J. Single-Cell RNA-Seq: Advances and Future Challenges. *Nucleic Acids Res.* **2014**, *42*, 8845−8860.
(8) Haque, A.; Engel, J.; Teichmann, S. A.; Lonnberg, T. A Practical Guide to Single-Cell RNA-Sequencing for Biomedical Research and Clinical Applications. *Genome Med.* **2017**, *9*, 75.
(9) Bertrand, E.; Chartrand, P.; Schaefer, M.; Shenoy, S. M.; Singer, R. H.; Long, R. M. Localization of Ash1 mRNA Particles in Living Yeast. *Mol. Cell* **1998**, *2*, 437−445.
(10) Paige, J. S.; Wu, K. Y.; Jaffrey, S. R. RNA Mimics of Green Fluorescent Protein. *Science* **2011**, *333*, 642−646.
(11) Neubacher, S.; Hennig, S. RNA Structure and Cellular Applications of Fluorescent Light-Up Aptamers. *Angew. Chem., Int. Ed.* **2019**, *58*, 1266−1279.
(12) Filonov, G. S.; Moon, J. D.; Svensen, N.; Jaffrey, S. R. Broccoli: Rapid Selection of an RNA Mimic of Green Fluorescent Protein by Fluorescence-Based Selection and Directed Evolution. *J. Am. Chem. Soc.* **2014**, *136*, 16299−16308.
(13) Bouhedda, F.; Fam, K. T.; Collot, M.; Autour, A.; Marzi, S.; Klymchenko, A.; Ryckelynck, M. A Dimerization-Based Fluorogenic Dye-Aptamer Module for RNA Imaging in Live Cells. *Nat. Chem. Biol.* **2020**, *16*, 69−76.
(14) Sunbul, M.; Lackner, J.; Martin, A.; Englert, D.; Hacene, B.; Grun, F.; Nienhaus, K.; Nienhaus, G. U.; Jaschke, A. Super-Resolution RNA Imaging Using a Rhodamine-Binding Aptamer with Fast Exchange Kinetics. *Nat. Biotechnol.* **2021**, *39*, 686−690.
(15) Gall, J. G.; Pardue, M. L. Formation and Detection of RNA-DNA Hybrid Molecules in Cytological Preparations. *Proc. Natl. Acad. Sci. U. S. A.* **1969**, *63*, 378−383.
(16) John, H. A.; Birnstiel, M. L.; Jones, K. W. RNA-DNA Hybrids at the Cytological Level. *Nature* **1969**, *223*, 582−587.
(17) Bauman, J. G.; Wiegant, J.; Borst, P.; van Duijn, P. A New Method for Fluorescence Microscopical Localization of Specific DNA Sequences by *in Situ* Hybridization of Fluorochromelabelled RNA. *Exp. Cell Res.* **1980**, *128*, 485−490.
(18) Langer-Safer, P. R.; Levine, M.; Ward, D. C. Immunological Method for Mapping Genes on Drosophila Polytene Chromosomes. *Proc. Natl. Acad. Sci. U. S. A.* **1982**, *79*, 4381−4385.
(19) Cui, C.; Shu, W.; Li, P. Fluorescence *in Situ* Hybridization: Cell-Based Genetic Diagnostic and Research Applications. *Front. Cell Dev. Biol.* **2016**, *4*, 89.
(20) Urbanek, M. O.; Krzyzosiak, W. J. RNA FISH for Detecting Expanded Repeats in Human Diseases. *Methods* **2016**, *98*, 115−123.
(21) Raj, A.; Rinn, J. L. Illuminating Genomic Dark Matter with RNA Imaging. *Cold Spring Harbor Perspect. Biol.* **2019**, *11*, a032094.
(22) Cui, C.; Shu, W.; Li, P. Fluorescence *in Situ* Hybridization: Cell-Based Genetic Diagnostic and Research Applications. *Front. Cell Dev. Biol.* **2016**, *4*, 89.
(23) Shaffer, S. M.; Joshi, R. P.; Chambers, B. S.; Sterken, D.; Biaesch, A. G.; Gabrieli, D. J.; Li, Y.; Feemster, K. A.; Hensley, S. E.; Issadore, D.; Raj, A. Multiplexed Detection of Viral Infections Using Rapid *in Situ* RNA Analysis on a Chip. *Lab Chip* **2015**, *15*, 3170−3182.
(24) Kwon, S. Single-Molecule Fluorescence *in Situ* Hybridization: Quantitative Imaging of Single RNA Molecules. *BMB Rep.* **2013**, *46*, 65−72.
(25) Shaffer, S. M.; Wu, M.-T.; Levesque, M. J.; Raj, A. Turbo FISH: A Method for Rapid Single Molecule RNA FISH. *PLoS One* **2013**, *8*, e75120.
(26) Femino, A.; Fay, F. S.; Fogarty, K.; Singer, R. H. Visualization of Single RNA Transcripts *in Situ*. *Science* **1998**, *280*, 585−590.
(27) Raj, A.; van den Bogaard, P.; Rifkin, S. A.; van Oudenaarden, A.; Tyagi, S. Imaging Individual mRNA Molecules Using Multiple Singly Labeled Probes. *Nat. Methods* **2008**, *5*, 877−879.
(28) Jensen, E. Technical Review: *In Situ* Hybridization. *Anat. Rec.* **2014**, *297*, 1349−1353.
(29) Sinnamon, J. R.; Czaplinski, K. RNA Detection *in Situ* with FISH-Stics. *RNA* **2014**, *20*, 260−266.
(30) Xia, C.; Babcock, H. P.; Moffitt, J. R.; Zhuang, X. Multiplexed Detection of RNA Using MerFISH and Branched DNA Amplification. *Sci. Rep.* **2019**, *9*, 7721.
(31) Wang, F.; Flanagan, J.; Su, N.; Wang, L. C.; Bui, S.; Nielson, A.; Wu, X.; Vo, H. T.; Ma, X. J.; Luo, Y. RNAscope: A Novel *in Situ* RNA Analysis Platform for Formalin-Fixed, Paraffin-Embedded Tissues. *J. Mol. Diagn.* **2012**, *14*, 22−29.
(32) Qing, Z. H.; Xu, J. Y.; Hu, J. L.; Zheng, J.; He, L.; Zou, Z.; Yang, S.; Tan, W. H.; Yang, R. H. *In Situ* Amplification-Based Imaging of RNA in Living Cells. *Angew. Chem., Int. Ed.* **2019**, *58*, 11574−11585.
(33) Lizardi, P. M.; Huang, X.; Zhu, Z.; Bray-Ward, P.; Thomas, D. C.; Ward, D. C. Mutation Detection and Single-Molecule Counting Using Isothermal Rolling-Circle Amplification. *Nat. Genet.* **1998**, *19*, 225−232.
(34) Choi, H. M. T.; Chang, J. Y.; Trinh, L. A.; Padilla, J. E.; Fraser, S. E.; Pierce, N. A. Programmable *in Situ* Amplification for Multiplexed Imaging of mRNA Expression. *Nat. Biotechnol.* **2010**, *28*, 1208−1212.
(35) Choi, H. M. T.; Beck, V. A.; Pierce, N. A. Next-Generation *in Situ* Hybridization Chain Reaction: Higher Gain, Lower Cost, Greater Durability. *ACS Nano* **2014**, *8*, 4284−4294.
(36) Kishi, J. Y.; Lapan, S. W.; Beliveau, B. J.; West, E. R.; Zhu, A.; Sasaki, H. M.; Saka, S. K.; Wang, Y.; Cepko, C. L.; Yin, P. Saber Amplifies FISH: Enhanced Multiplexed Imaging of RNA and DNA in Cells and Tissues. *Nat. Methods* **2019**, *16*, 533−544.
(37) Kishi, J. Y.; Schaus, T. E.; Gopalkrishnan, N.; Xuan, F.; Yin, P. Programmable Autonomous Synthesis of Single-Stranded DNA. *Nat. Chem.* **2018**, *10*, 155−164.
(38) Rouhanifard, S. H.; Mellis, I. A.; Dunagin, M.; Bayatpour, S.; Jiang, C. L.; Dardani, I.; Symmons, O.; Emert, B.; Torre, E.; Cote, A.; Sullivan, A.; Stamatoyannopoulos, J. A.; Raj, A. ClampFISH Detects Individual Nucleic Acid Molecules Using Click Chemistry−Based Amplification. *Nat. Biotechnol.* **2019**, *37*, 84−89.
(39) Orjalo, A.; Johansson, H. E.; Ruth, J. L. Stellaris Fluorescence *in Situ* Hybridization (FISH) Probes: A Powerful Tool for mRNA Detection. *Nat. Methods* **2011**, *8*, i−ii.
(40) Narrandes, S.; Xu, W. Gene Expression Detection Assay for Cancer Clinical Use. *J. Cancer* **2018**, *9*, 2249−2265.
(41) Huber, D.; Voith von Voithenberg, L.; Kaigala, G. V. Fluorescence *in Situ* Hybridization (FISH): History, Limitations and What to Expect from Micro-Scale FISH? *Micro Nano Eng.* **2018**, *1*, 15−24.
(42) Chinen, A. B.; Guan, C. M.; Ferrer, J. R.; Barnaby, S. N.; Merkel, T. J.; Mirkin, C. A. Nanoparticle Probes for the Detection of Cancer Biomarkers, Cells, and Tissues by Fluorescence. *Chem. Rev.* **2015**, *115*, 10530−10574.
(43) Wolfbeis, O. S. An Overview of Nanoparticles Commonly Used in Fluorescent Bioimaging. *Chem. Soc. Rev.* **2015**, *44*, 4743−4768.
(44) Howes, P. D.; Chandrawati, R.; Stevens, M. M. Colloidal Nanoparticles as Advanced Biological Sensors. *Science* **2014**, *346*, 1247390.
(45) Reisch, A.; Klymchenko, A. S. Fluorescent Polymer Nanoparticles Based on Dyes: Seeking Brighter Tools for Bioimaging. *Small* **2016**, *12*, 1968−1992.
(46) Algar, W. R.; Massey, M.; Rees, K.; Higgins, R.; Krause, K. D.; Darwish, G. H.; Peveler, W. J.; Xiao, Z.; Tsai, H.-Y.; Gupta, R.; Lix, K.; Tran, M. V.; Kim, H. Photoluminescent Nanoparticles for Chemical

https://doi.org/10.1021/acsnano.1c09409
ACS Nano XXXX, XXX, XXX−XXX

and Biological Analysis and Imaging. *Chem. Rev.* **2021**, *121*, 9243−9358.
(47) Luan, J.; Seth, A.; Gupta, R.; Wang, Z.; Rathi, P.; Cao, S.; Gholami Derami, H.; Tang, R.; Xu, B.; Achilefu, S.; Morrissey, J. J.; Singamaneni, S. Ultrabright Fluorescent Nanoscale Labels for the Femtomolar Detection of Analytes with Standard Bioassays. *Nat. Biomed. Eng.* **2020**, *4*, 518−530.
(48) Zhao, X. J.; Tapec-Dytioco, R.; Tan, W. H. Ultrasensitive DNA Detection Using Highly Fluorescent Bioconjugated Nanoparticles. *J. Am. Chem. Soc.* **2003**, *125*, 11474−11475.
(49) Hildebrandt, N.; Spillmann, C. M.; Algar, W. R.; Pons, T.; Stewart, M. H.; Oh, E.; Susumu, K.; Diaz, S. A.; Delehanty, J. B.; Medintz, I. L. Energy Transfer with Semiconductor Quantum Dot Bioconjugates: A Versatile Platform for Biosensing, Energy Harvesting, and Other Developing Applications. *Chem. Rev.* **2017**, *117*, 536−711.
(50) Wu, W. B.; Bazan, G. C.; Liu, B. Conjugated-Polymer-Amplified Sensing, Imaging, and Therapy. *Chem.* **2017**, *2*, 760−790.
(51) Melnychuk, N.; Egloff, S.; Runser, A.; Reisch, A.; Klymchenko, A. S. Light-Harvesting Nanoparticle Probes for FRET-Based Detection of Oligonucleotides with Single-Molecule Sensitivity. *Angew. Chem., Int. Ed.* **2020**, *59*, 6811−6818.
(52) Melnychuk, N.; Klymchenko, A. S. DNA-Functionalized Dye-Loaded Polymeric Nanoparticles: Ultrabright FRET Platform for Amplified Detection of Nucleic Acids. *J. Am. Chem. Soc.* **2018**, *140*, 10856−10865.
(53) Ochmann, S. E.; Vietz, C.; Trofymchuk, K.; Acuna, G. P.; Lalkens, B.; Tinnefeld, P. Optical Nanoantenna for Single Molecule-Based Detection of Zika Virus Nucleic Acids without Molecular Multiplication. *Anal. Chem.* **2017**, *89*, 13000−13007.
(54) Acuna, G. P.; Möller, F. M.; Holzmeister, P.; Beater, S.; Lalkens, B.; Tinnefeld, P. Fluorescence Enhancement at Docking Sites of DNA-Directed Self-Assembled Nanoantennas. *Science* **2012**, *338*, 506−510.
(55) Vafaei, S.; Allabush, F.; Tabaei, S. R.; Male, L.; Dafforn, T. R.; Tucker, J. H. R.; Mendes, P. M. Förster Resonance Energy Transfer Nanoplatform Based on Recognition-Induced Fusion/Fission of DNA Mixed Micelles for Nucleic Acid Sensing. *ACS Nano* **2021**, *15*, 8517−8524.
(56) He, D.; Wong, K.-W.; Dong, Z.; Li, H.-W. Recent Progress in Live Cell mRNA/MicroRNA Imaging Probes Based on Smart and Versatile Nanomaterials. *J. Mater. Chem. B* **2018**, *6*, 7773−7793.
(57) Prigodich, A. E.; Seferos, D. S.; Massich, M. D.; Giljohann, D. A.; Lane, B. C.; Mirkin, C. A. Nano-Flares for mRNA Regulation and Detection. *ACS Nano* **2009**, *3*, 2147−2152.
(58) Seferos, D. S.; Giljohann, D. A.; Hill, H. D.; Prigodich, A. E.; Mirkin, C. A. Nano-Flares: Probes for Transfection and mRNA Detection in Living Cells. *J. Am. Chem. Soc.* **2007**, *129*, 15477−15479.
(59) Briley, W. E.; Bondy, M. H.; Randeria, P. S.; Dupper, T. J.; Mirkin, C. A. Quantification and Real-Time Tracking of RNA in Live Cells Using Sticky-Flares. *Proc. Natl. Acad. Sci. U. S. A.* **2015**, *112*, 9591−9595.
(60) Zhou, W. J.; Li, D. X.; Xiong, C. Y.; Yuan, R.; Xiang, Y. Multicolor-Encoded Reconfigurable DNA Nanostructures Enable Multiplexed Sensing of Intracellular MicroRNAs in Living Cells. *ACS Appl. Mater. Interfaces* **2016**, *8*, 13303−13308.
(61) Li, N.; Wang, M. M.; Gao, X. N.; Yu, Z. Z.; Pan, W.; Wang, H. Y.; Tang, B. A DNA Tetrahedron Nanoprobe with Controlled Distance of Dyes for Multiple Detection in Living Cells and *in Vivo*. *Anal. Chem.* **2017**, *89*, 6670−6677.
(62) Chandrasekaran, A. R.; Punnoose, J. A.; Zhou, L.; Dey, P.; Dey, B. K.; Halvorsen, K. DNA Nanotechnology Approaches for MicroRNA Detection and Diagnosis. *Nucleic Acids Res.* **2019**, *47*, 10489−10505.
(63) He, L.; Lu, D.; Liang, H.; Xie, S.; Zhang, X.; Liu, Q.; Yuan, Q.; Tan, W. MRNA-Initiated, Three-Dimensional DNA Amplifier Able to Function inside Living Cells. *J. Am. Chem. Soc.* **2018**, *140*, 258−263.
(64) Ma, Y.; Mao, G.; Huang, W.; Wu, G.; Yin, W.; Ji, X.; Deng, Z.; Cai, Z.; Zhang, X.-E.; He, Z.; Cui, Z. Quantum Dot Nanobeacons for Single RNA Labeling and Imaging. *J. Am. Chem. Soc.* **2019**, *141*, 13454−13458.
(65) Liu, Y.; Le, P.; Lim, S. J.; Ma, L.; Sarkar, S.; Han, Z. Y.; Murphy, S. J.; Kosari, F.; Vasmatzis, G.; Cheville, J. C.; Smith, A. M. Enhanced MRNA FISH with Compact Quantum Dots. *Nat. Commun.* **2018**, *9*, 4461.
(66) Qu, A. H.; Sun, M. Z.; Xu, L. G.; Hao, C. L.; Wu, X. L.; Xu, C. L.; Kotov, N. A.; Kuang, H. Quantitative Zeptomolar Imaging of MiRNA Cancer Markers with Nanoparticle Assemblies. *Proc. Natl. Acad. Sci. U. S. A.* **2019**, *116*, 3391−3400.
(67) Pan, W.; Liu, B.; Gao, X. N.; Yu, Z. Z.; Liu, X. H.; Li, N.; Tang, B. A Graphene-Based Fluorescent Nanoprobe for Simultaneous Monitoring of MiRNA and MRNA in Living Cells. *Nanoscale* **2018**, *10*, 14264−14271.
(68) Dong, H.; Dai, W.; Ju, H.; Lu, H.; Wang, S.; Xu, L.; Zhou, S. F.; Zhang, Y.; Zhang, X. Multifunctional Poly(L-Lactide)-Polyethylene Glycol-Grafted Graphene Quantum Dots for Intracellular MicroRNA Imaging and Combined Specific-Gene-Targeting Agents Delivery for Improved Therapeutics. *ACS Appl. Mater. Interfaces* **2015**, *7*, 11015−11023.
(69) Kim, E.; Yang, J.; Park, J.; Kim, S.; Kim, N. H.; Yook, J. I.; Suh, J.-S.; Haam, S.; Huh, Y.-M. Consecutive Targetable Smart Nanoprobe for Molecular Recognition of Cytoplasmic MicroRNA in Metastatic Breast Cancer. *ACS Nano* **2012**, *6*, 8525−8535.
(70) Wang, Y.; Wu, C.; Chen, T.; Sun, H.; Cansiz, S.; Zhang, L.; Cui, C.; Hou, W.; Wu, Y.; Wan, S.; Cai, R.; Liu, Y.; Sumerlin, B. S.; Zhang, X.; Tan, W. DNA Micelle Flares: A Study of the Basic Properties That Contribute to Enhanced Stability and Binding Affinity in Complex Biological Systems. *Chem. Sci.* **2016**, *7*, 6041−6049.
(71) Dong, X.; Ong, S. Y.; Zhang, C.; Chen, W.; Du, S.; Xiao, Q.; Gao, L.; Yao, S. Q. Broad-Spectrum Polymeric Nanoquencher as an Efficient Fluorescence Sensing Platform for Biomolecular Detection. *ACS Sens.* **2021**, *6*, 3102−3111.
(72) Lin, L.-S.; Cong, Z.-X.; Cao, J.-B.; Ke, K.-M.; Peng, Q.-L.; Gao, J.; Yang, H.-H.; Liu, G.; Chen, X. Multifunctional Fe3o4@Polydopamine Core−Shell Nanocomposites for Intracellular MRNA Detection and Imaging-Guided Photothermal Therapy. *ACS Nano* **2014**, *8*, 3876−3883.
(73) Sahay, G.; Alakhova, D. Y.; Kabanov, A. V. Endocytosis of Nanomedicines. *J. Controlled Release* **2010**, *145*, 182−195.
(74) Iversen, T. G.; Skotland, T.; Sandvig, K. Endocytosis and Intracellular Transport of Nanoparticles: Present Knowledge and Need for Future Studies. *Nano Today* **2011**, *6*, 176−185.
(75) Patel, S.; Kim, J.; Herrera, M.; Mukherjee, A.; Kabanov, A. V.; Sahay, G. Brief Update on Endocytosis of Nanomedicines. *Adv. Drug Delivery Rev.* **2019**, *144*, 90−111.
(76) Ong, S. Y.; Zhang, C.; Xiao, D.; Yao, S. Q. Recent Advances in Polymeric Nanoparticles for Enhanced Fluorescence and Photoacoustic Imaging. *Angew. Chem., Int. Ed.* **2021**, *60*, 17797−17809.
(77) Reisch, A.; Didier, P.; Richert, L.; Oncul, S.; Arntz, Y.; Mely, Y.; Klymchenko, A. S. Collective Fluorescence Switching of Counterion-Assembled Dyes in Polymer Nanoparticles. *Nat. Commun.* **2014**, *5*, 4089.
(78) Reisch, A.; Trofymchuk, K.; Runser, A.; Fleith, G.; Rawiso, M.; Klymchenko, A. S. Tailoring Fluorescence Brightness and Switching of Nanoparticles through Dye Organization in the Polymer Matrix. *ACS Appl. Mater. Interfaces* **2017**, *9*, 43030−43042.
(79) Reisch, A.; Runser, A.; Arntz, Y.; Mely, Y.; Klymchenko, A. S. Charge-Controlled Nanoprecipitation as a Modular Approach to Ultrasmall Polymer Nanocarriers: Making Bright and Stable Nanoparticles. *ACS Nano* **2015**, *9*, 5104−5116.
(80) Reisch, A.; Heimburger, D.; Ernst, P.; Runser, A.; Didier, P.; Dujardin, D.; Klymchenko, A. S. Protein-Sized Dye-Loaded Polymer Nanoparticles for Free Particle Diffusion in Cytosol. *Adv. Funct. Mater.* **2018**, *28*, 1805157.
(81) Andreiuk, B.; Reisch, A.; Lindecker, M.; Follain, G.; Peyrieras, N.; Goetz, J. G.; Klymchenko, A. S. Fluorescent Polymer Nanoparticles for Cell Barcoding *in Vitro* and *in Vivo*. *Small* **2017**, *13*, 1701582.
(82) Trofymchuk, K.; Reisch, A.; Didier, P.; Fras, F.; Gilliot, P.; Mely, Y.; Klymchenko, A. S. Giant Light-Harvesting Nanoantenna for Single-Molecule Detection in Ambient Light. *Nat. Photonics* **2017**, *11*, 657.

https://doi.org/10.1021/acsnano.1c09409
ACS Nano XXXX, XXX, XXX−XXX

(83) Severi, C.; Melnychuk, N.; Klymchenko, A. S. Smartphone-Assisted Detection of Nucleic Acids by Light-Harvesting FRET-Based Nanoprobe. *Biosens. Bioelectron.* **2020**, *168*.112515
(84) Egloff, S.; Melnychuk, N.; Reisch, A.; Martin, S.; Klymchenko, A. S. Enzyme-Free Amplified Detection of Cellular MicroRNA by Light-Harvesting Fluorescent Nanoparticle Probes. *Biosens. Bioelectron.* **2021**, *179*, 113084.
(85) Melnychuk, N.; Ashokkumar, P.; Aparin, I. O.; Klymchenko, A. S. Pre- and Postfunctionalization of Dye-Loaded Polymeric Nanoparticles for Preparation of FRET-Based Nanoprobes. *ACS Appl. Mater. Interfaces* **2021**, DOI: 10.1021/acsapm.1c00819.
(86) Andreiuk, B.; Reisch, A.; Bernhardt, E.; Klymchenko, A. S. Fighting Aggregation-Caused Quenching and Leakage of Dyes in Fluorescent Polymer Nanoparticles: Universal Role of Counterion. *Chem. - Asian J.* **2019**, *14*, 836−846.
(87) Olie, R. A.; Simões-Wüst, A. P.; Baumann, B.; Leech, S. H.; Fabbro, D.; Stahel, R. A.; Zangemeister-Wittke, U. A Novel Antisense Oligonucleotide Targeting Survivin Expression Induces Apoptosis and Sensitizes Lung Cancer Cells to Chemotherapy. *Cancer Res.* **2000**, *60*, 2805−2809.
(88) Arvey, A.; Hermann, A.; Hsia, C. C.; Ie, E.; Freund, Y.; McGinnis, W. Minimizing Off-Target Signals in RNA Fluorescent *in Situ* Hybridization. *Nucleic Acids Res.* **2010**, *38*, e115.
(89) Thomsen, R.; Nielsen, P. S.; Jensen, T. H. Dramatically Improved RNA *in Situ* Hybridization Signals Using LNA-Modified Probes. *RNA* **2005**, *11*, 1745−1748.
(90) Floyd, D. L.; Ragains, J. R.; Skehel, J. J.; Harrison, S. C.; van Oijen, A. M. Single-Particle Kinetics of Influenza Virus Membrane Fusion. *Proc. Natl. Acad. Sci. U. S. A.* **2008**, *105*, 15382−15387.
(91) Karstens, T.; Kobs, K. Rhodamine B and Rhodamine 101 as Reference Substances for Fluorescence Quantum Yield Measurements. *J. Phys. Chem.* **1980**, *84*, 1871−1872.
(92) Texier, I.; Goutayer, M.; Da Silva, A.; Guyon, L.; Djaker, N.; Josserand, V.; Neumann, E.; Bibette, J.; Vinet, F. Cyanine-Loaded Lipid Nanoparticles for Improved *in Vivo* Fluorescence Imaging. *J. Biomed. Opt.* **2009**, *14*, 054005.

https://doi.org/10.1021/acsnano.1c09409
ACS Nano XXXX, XXX, XXX−XXX

Supporting information

Amplified Fluorescence *in Situ* Hybridization by Small and Bright Dye-Loaded Polymeric Nanoparticles

Sylvie Egloff,[§] Nina Melnychuk,[§] Elisabete Da Silva, Andreas Reisch, Sophie Martin, Andrey S. Klymchenko*

Laboratoire de Bioimagerie et Pathologies, UMR 7021 CNRS, Faculté de Pharmacie, Université de Strasbourg, 74, Route du Rhin, 67401 Illkirch, France.

[§] These authors contributed equally to this work.

*Corresponding author. E-mail address: andrey.klymchenko@unistra.fr (A. S. Klymchenko); tel: +33 368 85 42 55.

Table S1. Fluorescence quantum yields (QY) of NPs prepared with different dyes at varied loading mass ratio (*vs.* polymer).

Encapsulated dye	Loading mass ratio (%)[a]	QY (%)
R18/F5	30	52
	50	41
	70	32
Rh101-C18/F5	20	34
	30	21
	50	10
Rh101-C18/F12	20	46
	30	34
	50	18
DiD/F12	20	45
	30	42
	50	32

[a] The weight% loading of the dye with respect to the polymer.

Table S2. Sizes of bare and DNA-functionalized NPs according to TEM and DLS data.[a]

Dye	Type of NPs	Size by DLS	Size by TEM
Rh101-C18/F12	bare	17.0 ± 0.4	14.1 ± 1.8
	T20-NPs	23.4 ± 1.0	16.8 ± 2.0
R18/F5	bare	17.7 ± 0.4	18.2 ± 2.7
	T20-NPs	26.9 ± 0.3	20.0 ± 2.6
DiD/F12	bare	N/A	16.3 ± 2.3
	T20-NPs	N/A	17.9 ± 2.5

[a] Error bars are standard deviation of the mean ($n \geq 3$ for DLS; at least 200 NPs were analyzed for TEM).

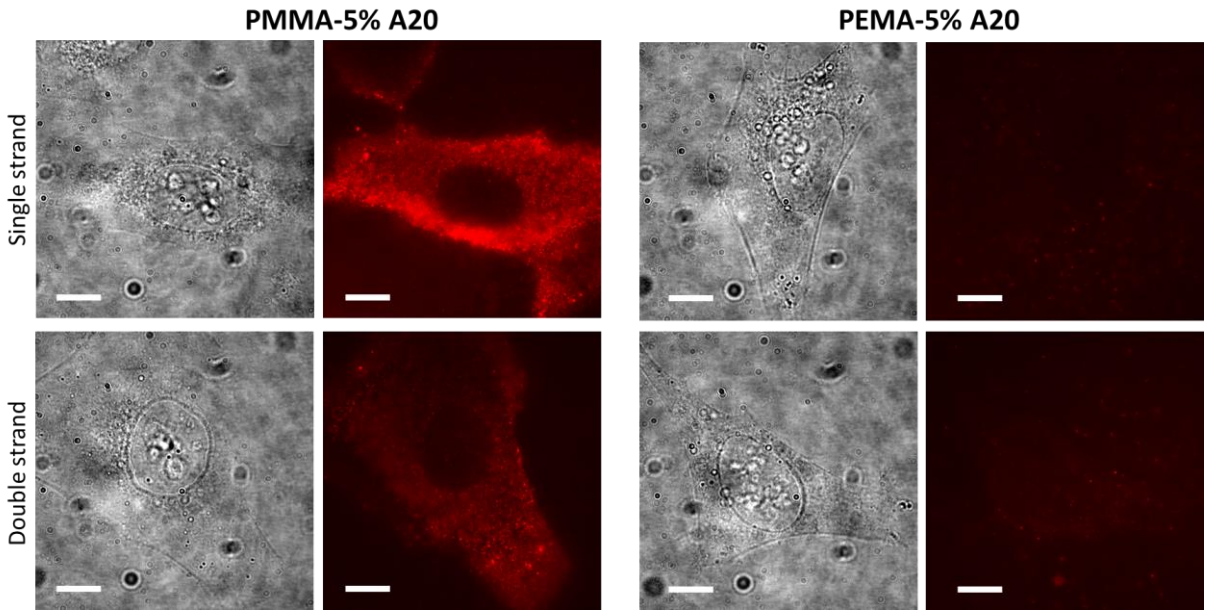

Figure S1. Effect of polymer nature and different grafted DNA sequences. Bright field (right) and fluorescence (left) images of fixed Hela cells incubated with PMMA-based NPs and PEMA-based NPs of ~20 nm core size, functionalized with A20. Both single-stranded and double stranded (annealed with T20) DNA-NPs were tested (30 min incubation with cells). TIRF mode was used on fixed Hela cells without washing. Scale bar: 10 μm. PBS buffer with 50 mg/L Tween 80 was used for incubation and imaging.

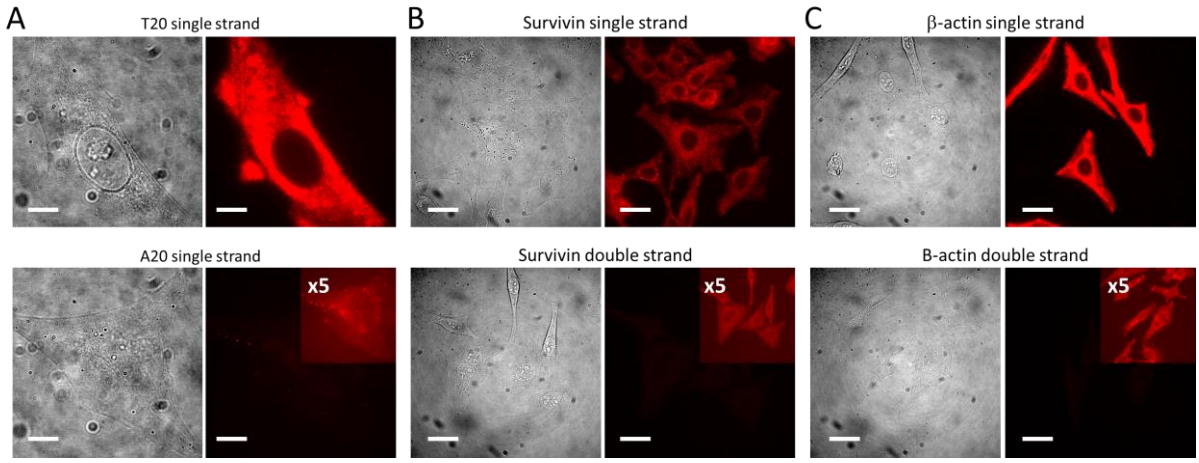

Figure S2. (A) Comparison of TIRF fluorescence images of PEMA-based NPs functionalized with T20 (upper panel) and A20 (lower panel) recorded at identical conditions (inset shows an image where signal was amplified 5-fold for visibility of the cell). Cells were incubated during 1 h with NPs, then washed two times with 0.1 % BSA / PBS. Scale bar: 10 μm. (B,C) Epi-fluorescence microscopy of fixed HeLa cells incubated for 1 h with DNA-NPs targeting survivin (B) and β-actin (C) (the same washing protocol as in A). Images for single-stranded (upper panels) and double-stranded (annealed with complementary strands) DNA-NPs are shown. Scale bar: 50 μm. PBS buffer with 50 mg/L Tween 80 was systematically used for incubation and imaging (A-C).

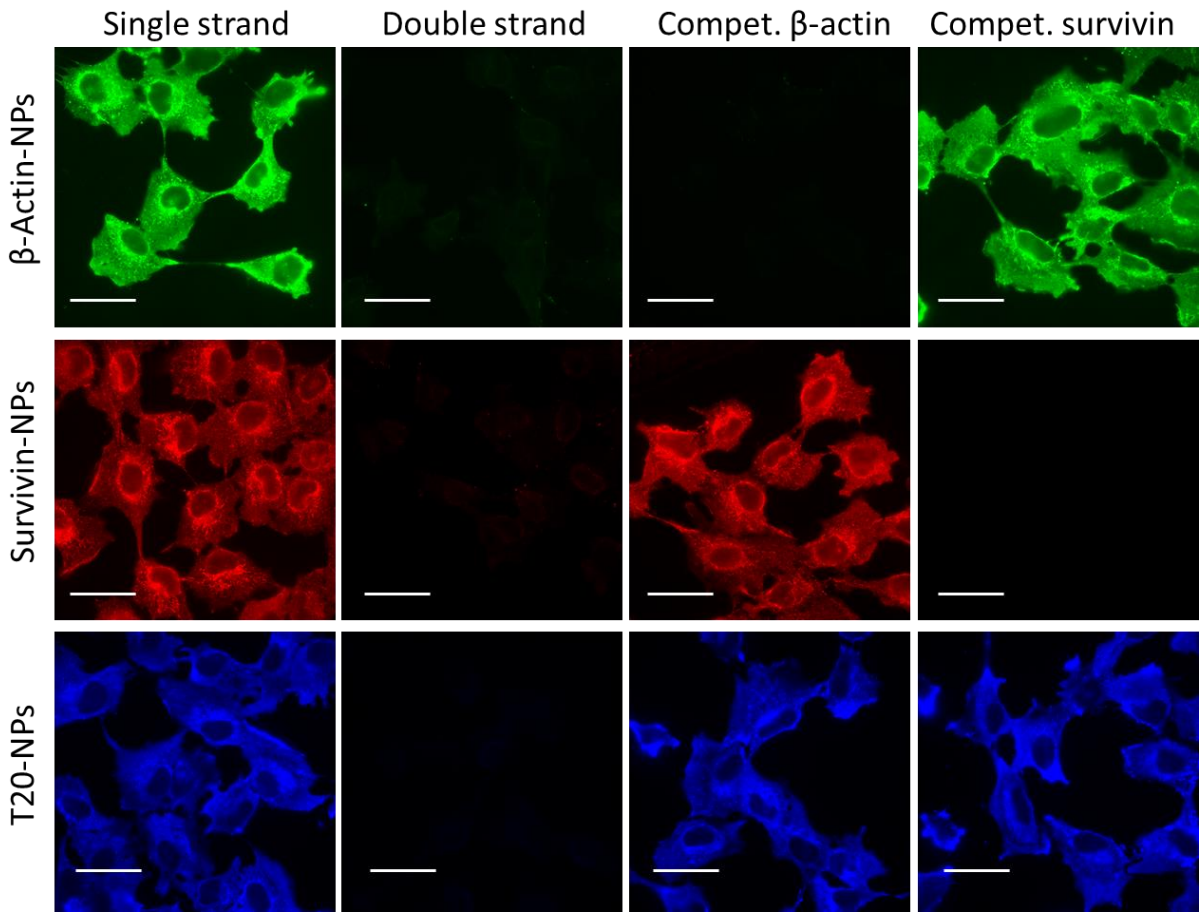

Figure S3. Validation of DNA-NPs for detection of intracellular mRNA targets in fixed U87 cells. Single stranded probes β-actin-NPs loaded with Rh110-C18/F12, survivin-NPs loaded with R18/F5 and A20-NPs loaded with DiD/F12 for β-actin, survivin and poly(A) sequences of mRNA, were compared to controls with double stranded DNA-NPs (annealed with complementary sequences) and competitor oligonucleotides (100 nM) for corresponding β-actin and survivin sequences added 1 h before addition of DNA NPs. DNA-NPs concentration expressed in encapsulated dyes was 100 nM. Scale bar: 50 μm.

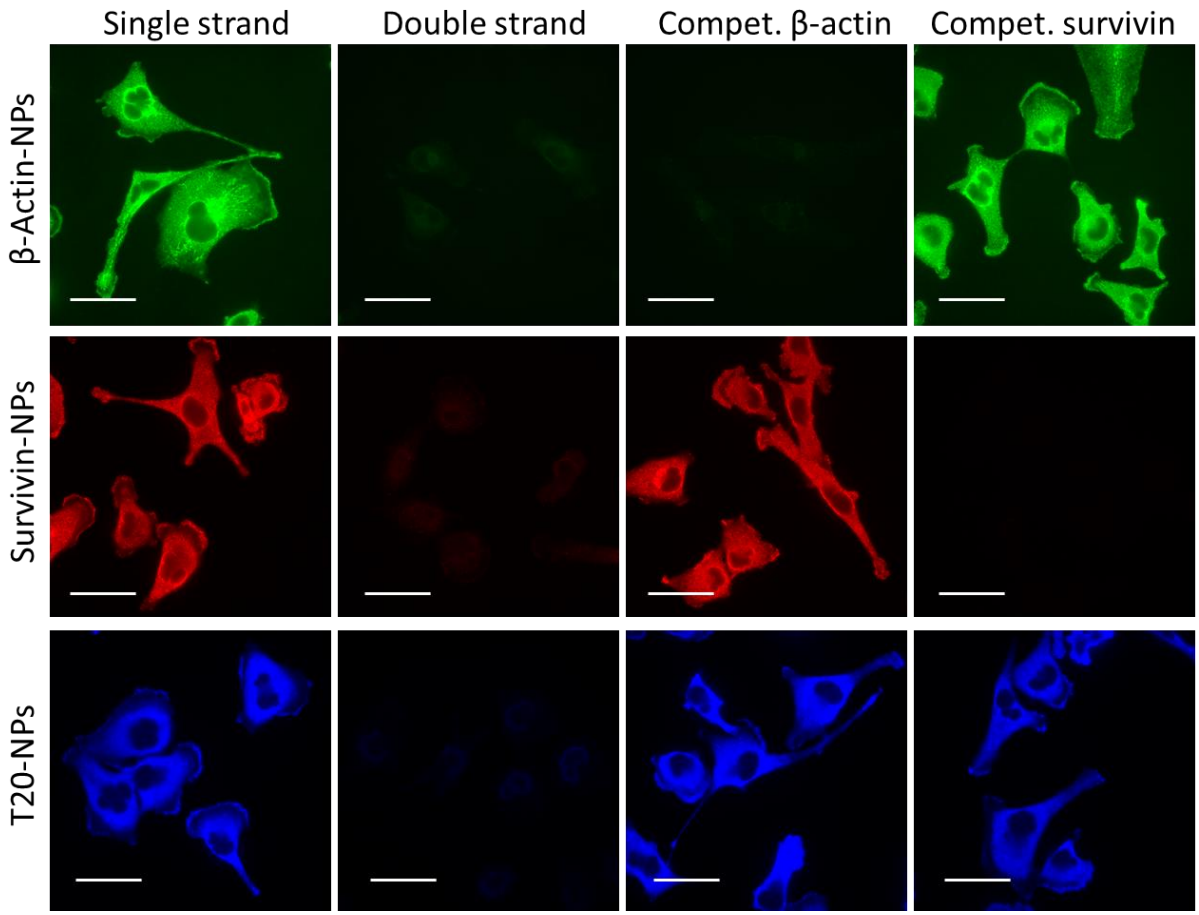

Figure S4. Validation of DNA-NPs for detection of intracellular mRNA targets in fixed MDA-MB-231 cells. Single stranded probes β-actin-NPs loaded with Rh110-C18/F12, survivin-NPs loaded with R18/F5 and A20-NPs loaded with DiD/F12 for β-actin, survivin and poly(A) sequences of mRNA, were compared to controls with double stranded DNA-NPs (annealed with complementary sequences) and competitor oligonucleotides (100 nM) for corresponding β-actin and survivin sequences added 1 h before addition of DNA NPs. DNA-NPs concentration expressed in encapsulated dyes was 100 nM. Scale bar: 50 μm.

Table S3. Manders' colocalization coefficient M1/M2 of multiplexed detection of mRNA sequences.

Colocalization	HeLa	U87	MDA
Actin in T20	0.988	0.935	0.998
T20 in Actin	0.322	0.208	0.283
Survivin in T20	0.937	0.750	0.962
T20 in Survivin	0.275	0.208	0.437
Actin in Survivin	0.661	0.499	0.946
Survivin in Actin	0.678	0.330	0.604

Supporting videos

Video S1. Video of 3D reconstruction of surviving mRNA imaging using AmpliFISH probes. HeLa cells were incubated during 1 h with DNA-NPs targeting survivin, then washed two times with 0.1 % BSA / PBS. Multiple stacks were acquired using spinning disk microscopy. 3D image reconstruction was performed using IMARIS software. Gray dots correspond to NPs identified automatically by the imaging software for quantitative analysis.

Video S2. Real-time video imaging of HeLa cells stained with actin-NPs using spinning disk fluorescence microscopy. HeLa cells were incubated during 1 h with DNA-NPs targeting β-actin mRNA, then washed two times with 0.1 % BSA / PBS. Multiple images from a single plane of HeLa cells was recorded each 100 ms using spinning disk microscopy. Scale bar is 10 µm.